

SUPPLEMENTARY INFORMATION

Cu(I) vs. Ru(II) photosensitizers: elucidation of electron transfer processes within a series of structurally related complexes containing an extended π -system

Ying Zhang,^{a,b} Philipp Traber,^a Linda Zedler,^b Stephan Kupfer,^a Stefanie Gräfe,^a Martin Schulz,^a Wolfgang Frey,^c Michael Karnahl,^{*c} Benjamin Dietzek^{*a,b,d}

^a Institute of Physical Chemistry and Abbe Center of Photonics, Friedrich Schiller University Jena, Helmholtzweg 4, 07743 Jena, Germany.

^b Department Functional Interfaces, Leibniz Institute of Photonic Technology Jena (IPHT), Albert-Einstein-Straße 9, 07745 Jena, Germany.

^c Institute of Organic Chemistry, University of Stuttgart, Pfaffenwaldring 55, 70569 Stuttgart, Germany.

^d Center for Energy and Environmental Chemistry, Friedrich Schiller University Jena, Lessingstrasse 10, 07743 Jena, Germany.

* Corresponding author. Dr. M. Karnahl, Tel: 0049-711-68564274, E-mail: michael.karnahl@oc.uni-stuttgart.de. Prof. Dr. B. Dietzek, Tel: 0049-3641-206332, E-mail: benjamin.dietzek@leibniz-ipht.de.

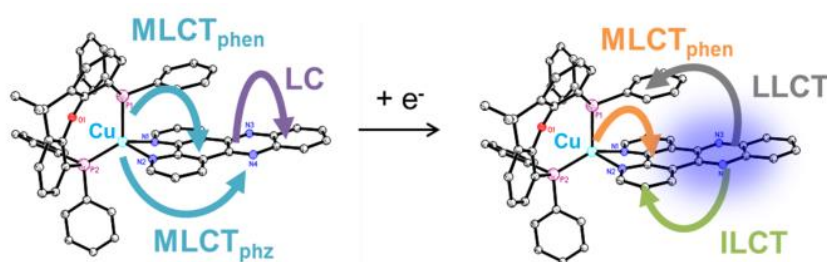


Table of Contents

1	Experimental details.....	S2
1.1	Characterization methods.....	S2
1.2	Computational details.....	S3
1.3	Synthetic details.....	S4
2	NMR and MS spectra of the complexes 1–3.....	S8
3	Crystallographic data and structures of the complexes 1 and 2.....	S10
4	Absorption spectra of complexes 1–4.....	S13
5	TDDFT calculations on 1–3 and 5–6.....	S14
6	UV-Vis-SEC on the redox of complexes 1–4.....	S30
7	RR data of complexes 1–7.....	S32
8	Reductive RR-SEC of complexes 1–7.....	S39

1 Experimental details

1.1 Characterization methods

NMR spectra were recorded either on a Bruker Avance III HD 400 or a Bruker Avance 500 at 298 K and processed with Bruker TopSpin software (version 3.2). The chemical shifts δ are given in parts per million (ppm). ^1H - and ^{13}C -NMR shifts are referenced to tetramethylsilane (TMS, $\delta = 0$ ppm). $^{31}\text{P}\{^1\text{H}\}$ -NMR shifts are proton decoupled and given relatively to H_3PO_4 (85 %, $\delta = 0$ ppm) as an external reference. Coupling constants J are given as absolute values in Hz, without considering the nature of the coupling. For the characterization of the NMR signals the following abbreviations are used: s = singlet, d = doublet, t = triplet, q = quartet, m = multiplet and dd = doublet of doublets.

ESI-MS values are given as m/z . Mass spectrometric measurements were conducted on a Bruker Daltonics micrOTOF-Q by the analytical service of the Institute of Organic Chemistry at the University of Stuttgart.

Elementary analysis (EA) was performed on dry and pulverized samples by the analytical service of the Institute of Organic Chemistry at the University of Stuttgart.

X-ray diffraction. Single-crystal X-ray diffraction analyses were carried out at 100 K on a Bruker Kappa APEXII Duo diffractometer with graphite-monochromated Mo K_α ($\lambda = 0.71073 \text{ \AA}$) or Cu K_α ($\lambda = 1.54178 \text{ \AA}$) radiation by using Omega-Phi scan technique¹. The structures were solved by direct methods using SHELXL97 software. ORTEP molecular graphics were performed by XP software². Crystal structures data were deposited at the Cambridge Crystallographic Data Centre with the respective deposition numbers CCDC1856414 (**1**) and CCDC1856415 (**2**).

Electrochemical measurements were carried out with a SP-150 potentiostat (Bio-Logic, France) in anhydrous acetonitrile (ACN) / 0.1 M TBAPF₆ solution using a three-electrode system, including UV-Vis-SEC, RR-SEC and CV measurements. The three-electrode system contains a Pt counter electrode, an Ag/AgCl pseudo-reference electrode and a glassy carbon working electrode for CVs. Argon was bubbled through the solution for 10 minutes prior to each measurement. The potentials were measured with respect to an Ag/AgCl reference electrode, and then ferrocenium/ferrocene (Fc^+/Fc) couple served as internal reference under the same experimental conditions. CVs were obtained at a scan rate of 100 mV/s.

UV-Vis absorption spectra were recorded on a double-beam V-670 spectrophotometer (JASCO, Japan) at room temperature. A standard 1 cm quartz cuvette was filled with 5–20 μM complexes **1–7** in various solvents. The ACN and dichloromethane (DCM) of spectroscopic grade were used without further purification. **Emission spectra** were measured with a Fluorolog-3 fluorimeter (Horiba, Japan) at room temperature. Complexes were dissolved in Ar-saturated solvents. The optical density was around 0.05 at the excitation wavelength in a

¹ Bruker. APEX2 and SAINT. Bruker AXS Inc., Madison, Wisconsin, USA, 2008.

² G. M. Sheldrick, *Acta Cryst.*, **2008**, A64, 112–122.

standard 1 cm quartz cuvette. The emission intensities were calibrated by the absorbance at the excitation wavelength and the Raman peaks of solvent are subtracted.

FT-Raman spectra were recorded using a MultiSpec spectrometer (Bruker, USA) with a spectral resolution of 1 cm^{-1} at room temperature. The Raman excitation light at 1064 nm was provided by a Nd:YAG laser (Klatsch DeniCAFC-LC-3/40) and the laser power at the sample was 50 mW. For each spectrum 200 scans were averaged. The Raman spectra showed no spectral changes over the measurement time. **Resonance Raman (RR) measurements** were performed through excitation by the visible lasers and detected by an IsoPlane 160 spectrometer (Princeton Instruments, USA) with an entrance slit width of 0.05 mm, a focal length of 750 mm, and grating 1200 or 2400 grooves/mm. The laser system contains a 405 nm diode laser (TopMode-405-HP, Toptica, Germany), a 473 nm diode pumped solid state lasers (HB-Laser, Germany), a 532 nm diode pumped solid state lasers (HB-Laser, Germany) and a 643 nm diode-pumped solid-state DL laser (CrystaLaser, USA). The excitation energy was attenuated to around 5 mW. The Raman signals were recorded by a thermoelectrically cooled PIXIS eXcelon camera (Princeton Instruments, USA). The Raman spectra were initially baseline corrected and normalized with respect to a solvent band, *i.e.*, to the signal at $920/1374\text{ cm}^{-1}$ for ACN. Subsequently the ACN spectrum was subtracted from the RR spectra.

UV-Vis absorption spectroelectrochemistry (UV-Vis-SEC) and Resonance Raman spectroelectrochemistry (RR-SEC) measurements were performed in a three-electrode thin-layer spectroelectrochemical cell with a pathlength of 1 mm. The setup was described before.^{3,4,5,6} A drilled glassy carbon piece served as the working electrode for UV-Vis-SEC and RR-SEC measurements. The “open circuit potential” spectrum (ocp) was initially recorded without externally applied potential. Subsequently, a given potential was applied by chronoamperometry. Simultaneously, the UV-Vis absorption spectra were recorded on a multichannel spectrometer (Avantes, the Netherlands) for UV-Vis-SEC. Similarly, the RR spectra were recorded prior to and during the chronoamperometry with the RR setup.

1.2 Computational details

All calculations were performed using Gaussian 16 Rev. B.01.⁷ Fully relaxed ground state geometries for all complexes (non-reduced: singlet and singly reduced: doublet) were obtained at the density functional level of

³ J. Schindler, Y. Zhang, P. Traber, J.-F. Lefebvre, S. Kupfer, M. Demeunynck, S. Gräfe, M. Chavarot-Kerlidou and B. Dietzek, *J. Phys. Chem. C*, **2018**, 122, 83–95.

⁴ Y. Zhang, S. Kupfer, L. Zedler, J. Schindler, T. Bocklitz, J. Guthmuller, S. Rau and B. Dietzek, *Phys. Chem. Chem. Phys.*, **2015**, 17, 29637–29646.

⁵ L. Zedler, J. Guthmuller, I. Rabelo de Moraes, S. Kupfer, S. Kriek, M. Schmitt, J. Popp, S. Rau and B. Dietzek, *Chem. Commun.*, **2014**, 50, 5227–5229.

⁶ L. Zedler, S. Kupfer, I. R. de Moraes, M. Wächtler, R. Beckert, M. Schmitt, J. Popp, S. Rau and B. Dietzek, *Chem. Eur. J.*, **2014**, 20, 3793–3799.

⁷ Gaussian 16, Revision B.01, M. J. Frisch, G. W. Trucks, H. B. Schlegel, G. E. Scuseria, M. A. Robb, J. R. Cheeseman, G. Scalmani, V. Barone, G. A. Petersson, H. Nakatsuji, X. Li, M. Caricato, A. V. Marenich, J. Bloino, B. G. Janesko, R. Gomperts, B. Mennucci, H. P. Hratchian, J. V. Ortiz, A. F. Izmaylov, J. L. Sonnenberg, D. Williams-Young, F. Ding, F. Lipparini, F. Egidi, J. Goings, B. Peng, A. Petrone, T. Henderson, D. Ranasinghe, V. G. Zakrzewski, J. Gao, N. Rega, G. Zheng, W. Liang, M. Hada, M. Ehara, K. Toyota, R. Fukuda, J. Hasegawa, M. Ishida, T. Nakajima, Y. Honda, O. Kitao, H. Nakai, T. Vreven, K. Throssell, J. A. Montgomery, Jr., J. E. Peralta, F.

theory (DFT) using the exchange-correlation hybrid functional B3LYP⁸ in combination with the def2SVPP (also known as def2-SV(P)) double- ζ basis set⁹ which uses an electronic core potential for the 28 lowest electrons of Ruthenium.¹⁰ To take dispersion effects into account, which are at least important for the Copper complexes **1** to **3**, Grimme's D3 dispersion correction with Becke-Johnson damping¹¹ was applied for all complexes. Solvent effects were considered by the integral equation formalism of the polarizable continuum model (IEFPCM)¹² for ACN. To verify the ground state being a local minimum of the 3N-6 potential energy hypersurface frequency calculations were performed. Excited state properties, as are excitation energies, transition dipole moments and electric characters were obtained using the same computational setup as the preliminary ground state calculations via time-dependent DFT (TDDFT). The lowest 100 excited states were calculated for each redox state (non-reduced: singlet and singly reduced: doublet) of each structure, respectively. Additionally, the gradients of bright excited states were calculated for the non-reduced and singly reduced complexes. The non-equilibrium procedure of solvation was used for the calculation of the excitation energies, transition dipole moments and excited state gradients within the Franck-Condon region, which is well adapted for processes where only the fast reorganization of the electronic distribution of the solvent is important. The RR intensities were obtained using a local code using the sum-over-states formalism; detailed information on the computational method can be found in Refs [13,14]. A homogeneous broadening given by $\Gamma = 1500 \text{ cm}^{-1}$ was applied for all RR calculation in resonance with the excitation wavelengths as utilized in the RR experiments. The Cube files for the molecular orbitals as well as for the electron densities, the hole densities and the charge density differences were computed using Multiwfn 3.5¹⁵ and imaged using UCSF Chimera 1.11.¹⁶

1.3 Synthetic details

The Cu(I) precursor $[\text{Cu}(\text{ACN})_4]\text{PF}_6$ (ACN = acetonitrile), xantphos (xant) and all starting materials of the different diimine ligands (e.g. 1,10-phenanthroline (phen) and 2,9-dimethyl-1,10-phenanthroline (dmp)) were purchased from commercial suppliers and used without further purification. If not stated otherwise, all preparations of the Cu(I) compounds were conducted under nitrogen atmosphere by using standard Schlenk

Ogliaro, M. J. Bearpark, J. J. Heyd, E. N. Brothers, K. N. Kudin, V. N. Staroverov, T. A. Keith, R. Kobayashi, J. Normand, K. Raghavachari, A. P. Rendell, J. C. Burant, S. S. Iyengar, J. Tomasi, M. Cossi, J. M. Millam, M. Klene, C. Adamo, R. Cammi, J. W. Ochterski, R. L. Martin, K. Morokuma, O. Farkas, J. B. Foresman, and D. J. Fox, Gaussian, Inc., Wallingford CT, **2016**.

⁸ a) A. D. Becke, *J. Chem. Phys.*, **1993**, 98, 5648-5652; b) A. D. Becke, *Phys. Rev. A*, **1988**, 38, 3098; c) S. H. Vosko, L. Wilk, M. Nusair, *Canadian Journal of Physics*, **1980**, 58, 1200-1211; d) P. J. Stephens, F. J. Devlin, C. F. Chabalowski, M. J. Frisch, *J. Phys. Chem.*, **1994**, 98, 11623-11627; e) Lee, C.; Yang, W.; Parr, R. G. *Phys Rev B*, **1988**, 37, 785-789.

⁹ F. Weigend, R. Ahlrichs, *Phys. Chem. Chem. Phys.*, **2005**, 7, 3297-3305.

¹⁰ D. Andrae, U. Häußermann, M. Dolg, H. Stoll, H. Preuß, *Theoret. Chim. Acta*, **1990**, 77, 123-141.

¹¹ S. Grimme, S. Ehrlich, L. Goerigk, *J. Comp. Chem.*, **2011**, 32, 1456-65.

¹² B. Mennucci, C. Cappelli, C. A. Guido, R. Cammi, J. Tomasi, *J. Phys. Chem. A*, **2009**, 113, 3009-3020.

¹³ M. Wächtler, J. Guthmüller, L. González, B. Dietzker, *Coord. Chem. Rev.* **2012**, 256 (15-16), 1479-1508

¹⁴ J. Guthmüller, *J. Chem. Phys.* **2016**, 064106.

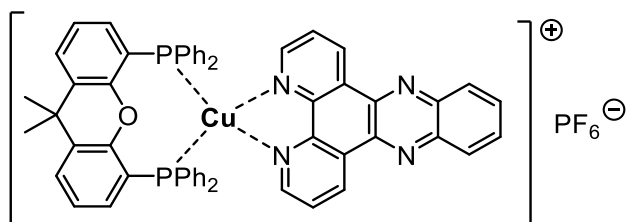
¹⁵ T. Lu, F. Chen, *J. Comput. Chem.*, **2012**, 33, 580-592.

¹⁶ E. F. Pettersen, T. D. Goddard, C. C. Huang, G. S. Couch, D. M. Greenblatt, E. C. Meng, T. E. Ferrin, *J. Comput. Chem.*, **2004**, 25, 1605-1612.

techniques. Solvents were purified and dried according to conventional procedures.¹⁷ The heteroleptic copper complexes were synthesized by a one-pot two-step procedure as previously described in literature.^{18,19,20}

Dipyrido[3,2-f:2',3'-h]quinoxaline (dpq), dipyrido[3,2-a:2',3'-c]phenazine (dppz), 3,6,11,12-tetramethyl-dipyrido[3,2-a:2',3'-c]phenazine (tmdppz) and [Cu(xant)(dmp)]PF₆ (**4**) were synthesized according to literature and matched all reported characterization.^{21,22,23} The already known Ru(II) complexes **5–7** (see Figure S1) were also prepared according to literature methods.^{24,25}

[Cu(xant)(dppz)]PF₆ (**1**)



132 mg (0.35 mmol) of [Cu(ACN)₄]PF₆ and 205 mg of xantphos (0.35 mmol) were placed into a dry flask under N₂ atmosphere and dissolved in 15 mL of dry DCM. The mixture was then stirred for 20 h under reflux. A solution of 201 mg dppz (0.35 mmol) in 5 mL of dry DCM was added to the reaction mixture at room temperature. The yellow mixture was refluxed for 3 h, cooled to ambient temperature and eventually added NH₄PF₆ and *n*-hexane. The precipitation was filtered off, washed with *n*-hexane, H₂O and Et₂O. After drying *in vacuo* the title compound was received as a yellow solid in 57 % yield (211 mg, 0.20 mmol).

¹H-NMR (400 MHz, CD₃CN): δ (ppm) = 9.68 (dd, *J* = 1.3, 8.2, 2H), 8.62 (s, 2H), 8.45 (dd, *J* = 3.4, 6.5, 2H), 8.10 (dd, *J* = 3.4, 6.5, 2H), 7.86 (dd, *J* = 4.8, 8.2, 2H), 7.82 (dd, *J* = 1.3, 7.8, 2H), 7.28-6.95 (m, 22 H), 6.67-6.61 (m, 2H), 1.78 (s, 6H). ¹³C-NMR (125 MHz, CD₃CN): δ (ppm) = 154.5, 142.4, 132.49, 132.23, 132.37, 130.7, 129.7, 129.2, 128.51, 128.47, 128.43, 127.6, 124.9, 27.2. ³¹P-NMR (161 MHz, CD₃CN): δ (ppm) = -12.76. (+)ESI-MS (high resolution) *m/z*: calcd. for [C₅₇H₄₂CuN₄OP₂]⁺: 923.2124, found: 923.2101 [M]⁺. EA calcd. for C₅₇H₄₂CuF₆N₄OP₃: C (calcd: 64.02, found: 63.90), H (calcd: 3.96, found: 4.19), N (calcd: 5.24, found: 5.53).

Crystals suitable for X-ray crystallography were received from a saturated DCM/*n*-hexane solution (see below).

¹⁷ L. A. Wilfred, L. L. C. Christina, *Purification of Laboratory Chemicals* (Sixth Edition), Butterworth-Heinemann, Oxford, **2009**.

¹⁸ S.-P. Luo, E. Mejía, A. Friedrich, A. Pazidis, H. Junge, A.-E. Surkus, R. Jackstell, S. Denurra, Gladiali, S. Lochbrunner, M. Beller, *Angew. Chem.*, **2013**, 125, 437-441.

¹⁹ E. Mejía, S.-P. Luo, M. Karnahl, A. Friedrich, S. Tschierlei, A.-E. Surkus, H. Junge, S. Gladiali, S. Lochbrunner, M. Beller, *Chem. Eur. J.*, **2013**, 19, 15972-15978

²⁰ M. Heberle, S. Tschierlei, N. Rockstroh, M. Ringenberg, W. Frey, H. Junge, M. Beller, S. Lochbrunner, M. Karnahl, *Chem. Eur. J.*, **2017**, 23, 312-319.

²¹ C. Kuhnt, M. Karnahl, S. Tschierlei, K. Griebenow, M. Schmitt, B. Schäfer, S. Kriek, H. Görls, S. Rau, B. Dietzek, J. Popp, *Phys. Chem. Chem. Phys.*, **2010**, 12, 1357-1368.

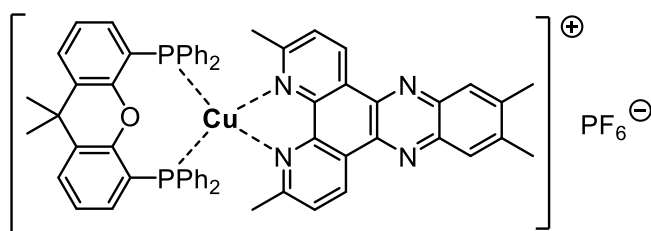
²² R. M. Hartshorn, J. K. Barton, *J. Am. Chem. Soc.*, **1992**, 114, 5919-5925.

²³ Y. Zhang, M. Heberle, M. Wächtler, M. Karnahl, B. Dietzek, *RSC Advances*, **2016**, 6, 105801-105805.

²⁴ E. Amouyal, A. Homsy, J. Chambron, J. Sauvage, *J. Chem. Soc., Dalton Trans.*, **1990**, 1841-1845.

²⁵ S. Rau, B. Schäfer, A. Grüßing, S. Schebesta, K. Lamm, J. Vieth, H. Görls, D. Walther, M. Rudolph, U. W. Grummt, E. Birkner, *Inorg. Chim. Acta*, **2004**, 357, 4496-4503.

[Cu(xant)(tmdppz)]PF₆ (2)

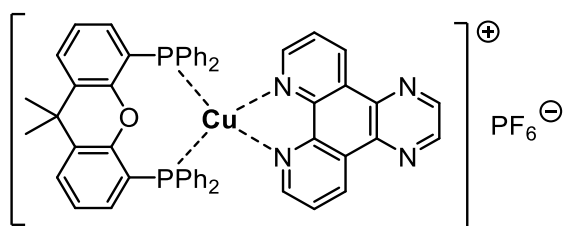


102 mg (0.27 mmol) of [Cu(ACN)₄]PF₆ and 158 mg of xantphos (0.27 mmol) were placed into a dry Schlenk flask under N₂ atmosphere. After dissolving in 20 mL dry DCM the mixture was stirred for 20 h under reflux. A solution of Me₂dppzMe₂ in 5 mL of dry DCM was added to the reaction mixture at ambient temperature. After refluxing for further 3 h, the mixture was cooled to room temperature, concentrated under reduced pressure. Then NH₄PF₆ and finally *n*-hexane were added at 0 °C to precipitate a bright yellow solid. The solid was filtered off, carefully washed with *n*-hexane, H₂O and Et₂O. The solid compound was dried *in vacuo* to receive the complex in 66 % yield (202 mg, 0.18 mmol).

¹H-NMR (500 MHz, CD₃CN): δ (ppm) = 9.33 (d, *J* = 8.3 Hz, 2H), 8.03 (s, 2H), 7.62 (d, *J* = 8.3 Hz, 2H), 7.30-6.97 (m, 26H), 2.61 (s, 6H), 2.29 (s, 6H), 1.73 (s, 6H). ¹³C-NMR (125 MHz, CD₃CN): δ (ppm) = 160.1, 154.5, 144.3, 142.9, 141.4, 138.2, 133.9, 133.6, 132.72, 132.66, 132.60, 131.1, 129.9, 129.6, 128.6, 128.41, 128.37, 128.34, 127.9, 127.7, 127.5, 126.3, 125.9, 125.1, 35.6, 27.6, 26.4, 20.1, 19.4. ³¹P-NMR (202 MHz, CD₃CN): δ (ppm) = -12.81. (+)ESI-MS (high resolution) *m/z*: calcd. for [C₆₁H₅₀CuN₄OP₂]⁺: 979.2750, found: 979.2763 [M]⁺.

Crystals suitable for X-ray crystallography were again received from a saturated DCM/*n*-hexane solution (see below).

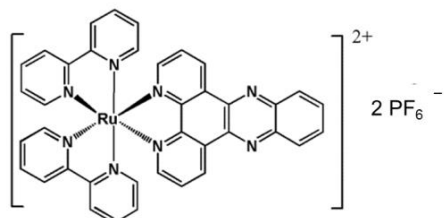
[Cu(xant)(dpq)]PF₆ (3)



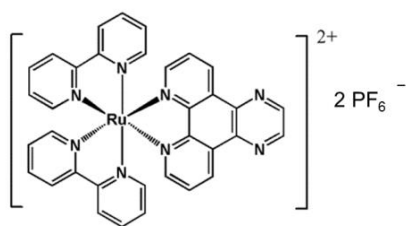
160 mg (0.43 mmol) of [Cu(ACN)₄]PF₆ and 249 mg of xantphos (0.43 mmol) were placed into a dry Schlenk flask under N₂ atmosphere. After dissolving in 20 mL of dry DCM the mixture was stirred for 20 h under reflux. Then a solution containing 100 mg (0.43 mmol) of the dpq ligand in 5 mL dry DCM was added to the reaction mixture at ambient temperature. After refluxing for further 3 h, the mixture was cooled to room temperature. The precipitate was filtered off and NH₄PF₆ as well as *n*-hexane were added to the clear yellow filtrate. The yellow precipitation was filtered off, washed with *n*-hexane, H₂O and Et₂O. After drying *in vacuo* the title compound was received as a yellow solid in 77 % yield (337 mg, 0.33 mmol).

¹H-NMR (400 MHz, CD₃CN): δ (ppm) = 9.56 (dd, *J* = 1.4, 8.3, 2H), 9.17 (s, 2H), 8.62 (s, 2H), 7.85 (dd, *J* = 4.8, 8.3, 2H), 7.81 (dd, *J* = 1.0, 7.8, 2H), 7.26-6.92 (m, 21 H), 6.66-6.59 (m, 2H), 1.78 (s, 6H). ¹³C-NMR (125 MHz, CD₃CN):

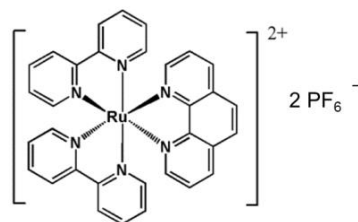
δ (ppm) = 134.2, 132.6, 130.9, 129.8, 128.64, 128.60, 128.57, 127.7, 125.0, 27.3. $^{31}\text{P-NMR}$ (161 MHz, CD_3CN):
 δ (ppm) = -12.38. (+)ESI-MS (high resolution) m/z : calcd. for $[\text{C}_{53}\text{H}_{40}\text{CuN}_4\text{OP}_2]^+$: 873.1968, (found): 873.1989
 $[\text{M}]^+$. EA calcd. for $[\text{C}_{53}\text{H}_{40}\text{CuF}_6\text{N}_4\text{OP}_3] \cdot 2\text{H}_2\text{O}$: C (calcd: 60.32, found: 60.67), H (calcd: 4.20, found: 4.09), N (calcd:
5.31, found: 5.76).



[Ru(bpy)₂(dppz)](PF₆)₂ (5)



[Ru(bpy)₂(dpq)](PF₆)₂ (6)



[Ru(bpy)₂(phen)](PF₆)₂ (7)

Figure S1. Structures of the Ru(II) complexes 5–7.

2 NMR and MS spectra of the complexes 1–3

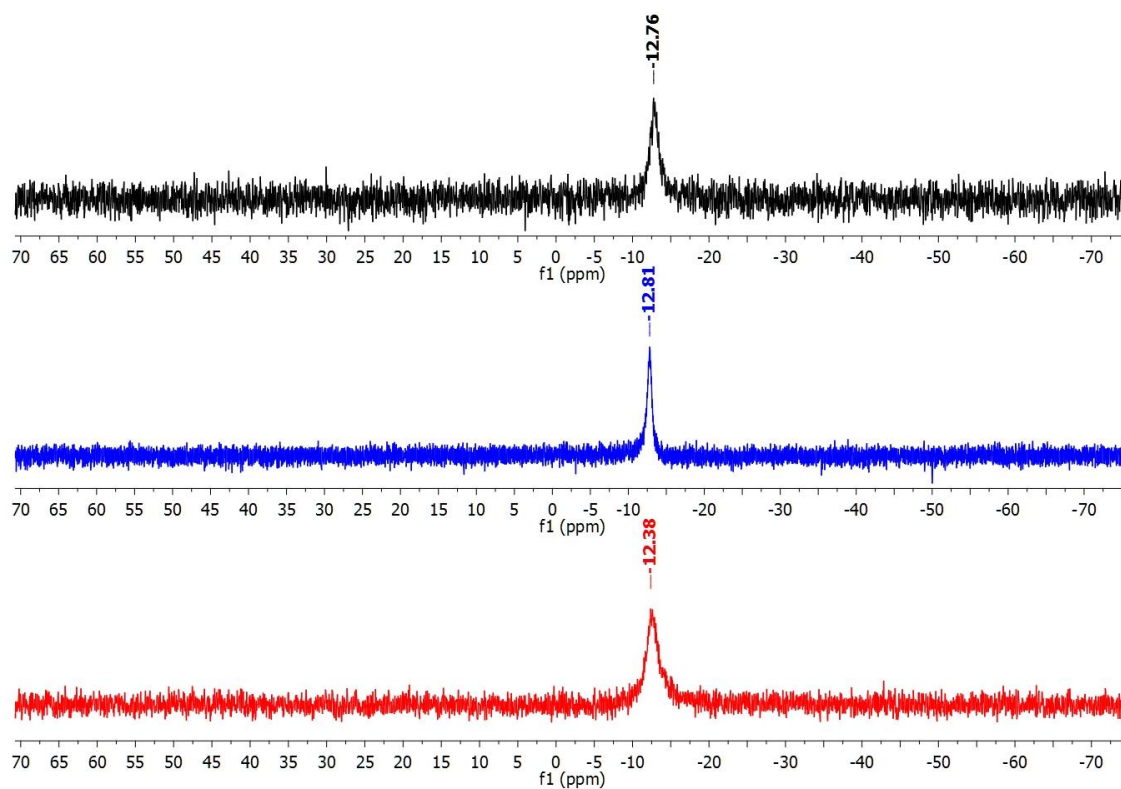


Figure S2. Comparison of the $^{31}\text{P}\{^1\text{H}\}$ -NMR spectra of the heteroleptic copper complexes **1** (black), **2** (blue) and **3** (red) in CD_3CN . It becomes obvious that there is almost no change in the chemical shift within this series of complexes.

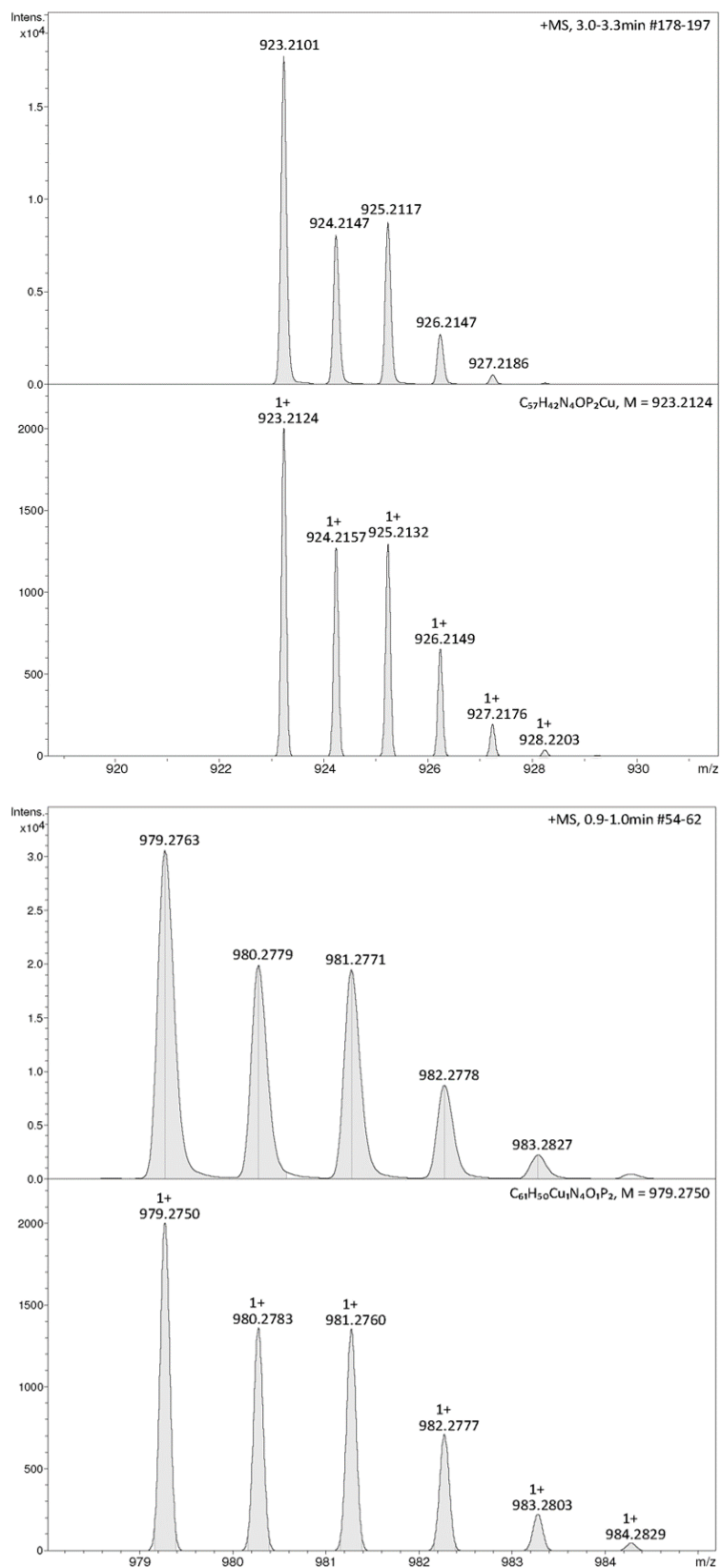


Figure S3. High resolution (+)-ESI mass spectra of the heteroleptic Cu(I) complexes **1** (top) and **2** (bottom) with matching isotopic pattern.

3 Crystallographic data and structures of the complexes 1 and 2

Table S1. Crystallographic data and refinement details of the complexes 1 and 2.

Compound	1	2
CCDC number [#]	1856414	1856415
Empirical formula	C ₆₃ H ₅₁ CuF ₆ N ₇ OP ₃	C _{63.25} H _{55.5} Cl _{0.50} CuF ₆ N ₄ O _{1.5} OP ₃
Formula weight	1192.56	1183.79
Temperature (K)	240(2)	130(2)
Wavelength (Å)	0.71073	1.54178
Crystal system, space group	Monoclinic, P 21/n	Triclinic, P -1
Unit cell dimensions (Å, °)		
a	11.440(4)	12.3503(18)
α	90	102.835(13)
b	28.561(9)	21.560(3)
β	107.390(14)	94.635(12)
c	18.045(6)	23.198(4)
γ	90	95.324(12)
Volume (Å ³)	5627(3)	5963.9(16)
Z, calculated density (Mg m ⁻³)	4, 1.408	4, 1.318
Absorption coefficient (mm ⁻¹)	0.543	2.018
F(000)	2456	2446
Crystal size (mm)	0.31 x 0.15 x 0.09	0.11 x 0.08 x 0.03
Theta range for data collection (°)	1.38 to 26.50	4.23 to 64.00
Limiting indices	-13<=h<=14, -35<=k<=35, 20<=l<=22	-12<=h<=14, -25<=k<=21, -27<=l<=26
Reflections collected / unique	81001 / 11525 [R(int) = 0.1074]	54587 / 19142 [R(int) = 0.1450]
Completeness of data	98.8 % (Theta: 26.50°)	96.6 % (Theta: 64.00°)
Absorption correction	semi-empirical from equivalents	semi-empirical from equivalents
Max. and min. transmission	0.7308 and 0.6649	0.7528 and 0.6310
Refinement method	Full-matrix least-squares on F ²	Full-matrix-block least-squares on F ²
Data / restraints / parameters	11525 / 90 / 780	19142 / 280 / 1556
Goodness-of-fit on F ²	1.053	1.050
Final R indices [I > 2σ(I)]	R1 = 0.0508, wR2 = 0.0991	R1 = 0.0916, wR2 = 0.1957
R indices (all data)	R1 = 0.1092, wR2 = 0.1108	R1 = 0.1926, wR2 = 0.2269
Extinction coefficient		0.00048(5)
Largest diff. peak and hole (e.Å ⁻³)	0.406 and -0.382	1.199 and -0.604

[#] CCDC 1856414 (1) and 1856415 (2) contain the supplementary crystallographic data for this paper. These data are provided free of charge by The Cambridge Crystallographic Data Centre.

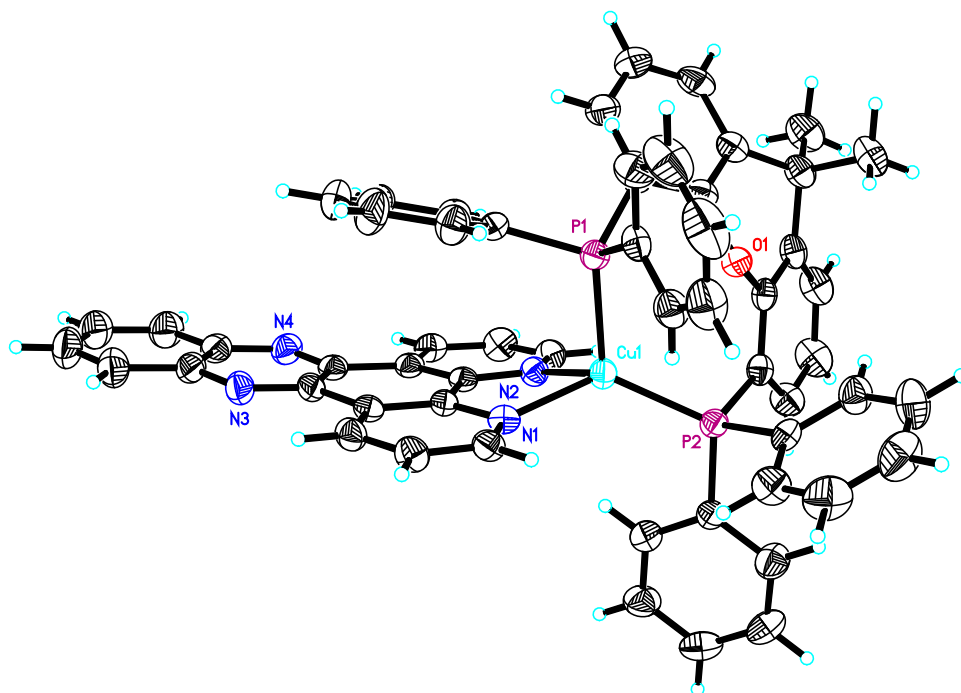


Figure S4. Solid state structure (ORTEP representation) of complex **1** with thermal ellipsoids at a probability level of 50 %. The PF_6^- counter anion and solvent molecules are omitted for clarity. In contrast to the main text in this visualization all hydrogen atoms are shown and the orientation of **1** is changed to allow for another point of view.

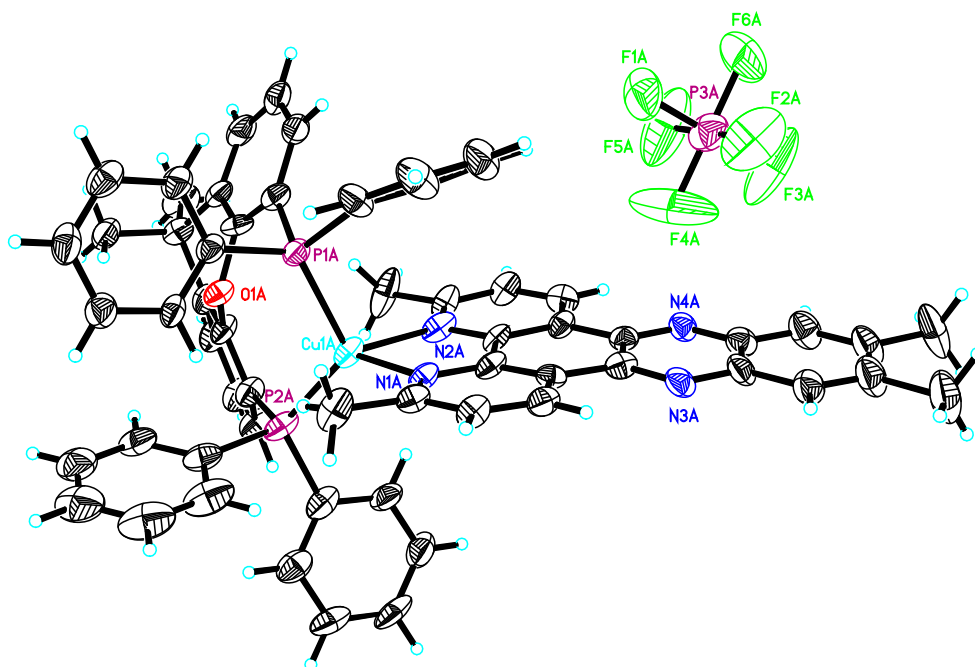


Figure S5. Solid state structure (ORTEP representation) of complex **2** with thermal ellipsoids at a probability level of 50 %. Solvent molecules are omitted for clarity.

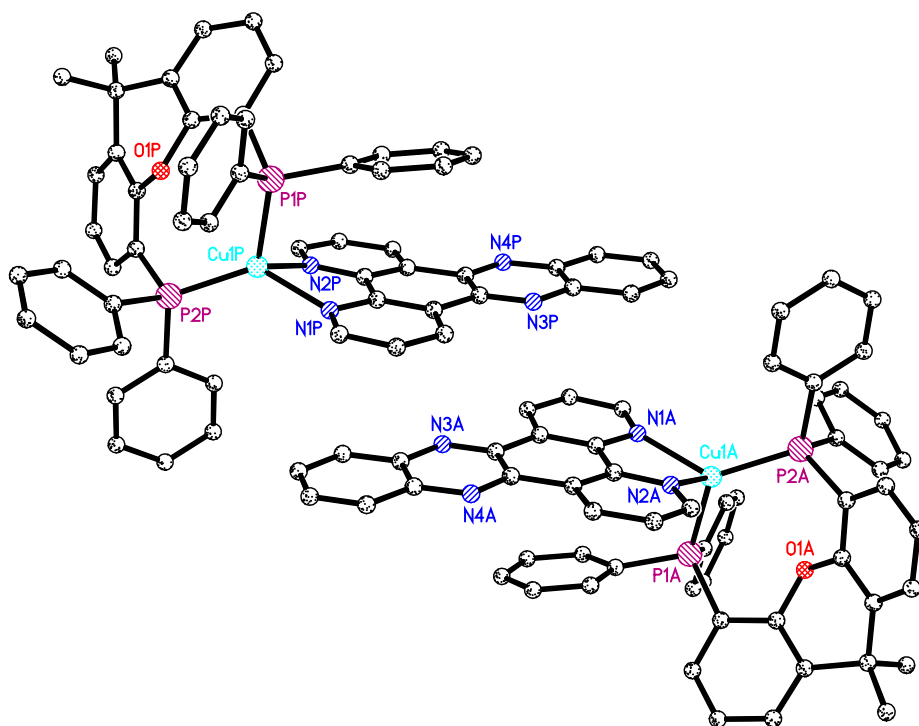


Figure S6. Arrangement of two neighboring complexes of compound **1** in the solid state. The phenanthroline part of the dppz ligand stacks with the phenazine part of the second dppz in a centrosymmetric fashion. Distances of around 3.5 to 3.8 Å between the two dppz ligands are indicative for weak intermolecular π - π interactions.

Table S2. Selected crystallographic bond lengths (Å) and angles (°) of the Cu(I) complexes **1** and **2**. The data of the reference complex **4** is given for comparison and taken from literature.²⁶

Compound	1	2	4
Diimine ligand	dppz	tmdppz	dmp
Cu-N1	2.097(3)	2.099(6)	2.084(3)
Cu-N2	2.069(2)	2.106(6)	2.112(3)
Cu-P1	2.2857(10)	2.283(2)	2.2626(11)
Cu-P2	2.2311(10)	2.253(2)	2.2863(13)
N1-Cu-N2	79.86(9)	79.8(2)	80.53(13)
P1-Cu-P2	120.02(3)	115.85(8)	112.93(4)
N1-Cu-P1	97.42(6)	104.13(15)	108.77(9)
N1-Cu-P2	131.69(7)	126.49(17)	120.33(9)
N2-Cu-P1	105.88(7)	109.15(17)	120.33(9)
N2-Cu-P2	113.67(7)	115.65(17)	118.59(9)

²⁶ M. Heberle, S. Tschierlei, N. Rockstroh, M. Ringenberg, W. Frey, H. Junge, M. Beller, S. Lochbrunner, M. Karnahl, *Chem. Eur. J.*, **2017**, *23*, 312-319.

4 Absorption spectra of complexes 1–4

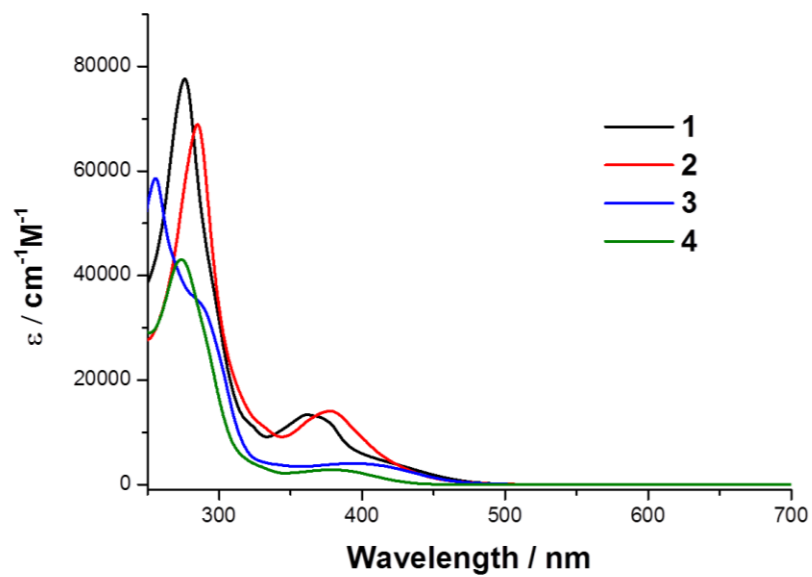


Figure S7. UV-Vis absorption spectra of the complexes 1–4 in DCM.

5 TDDFT calculations on 1–3 and 5–6

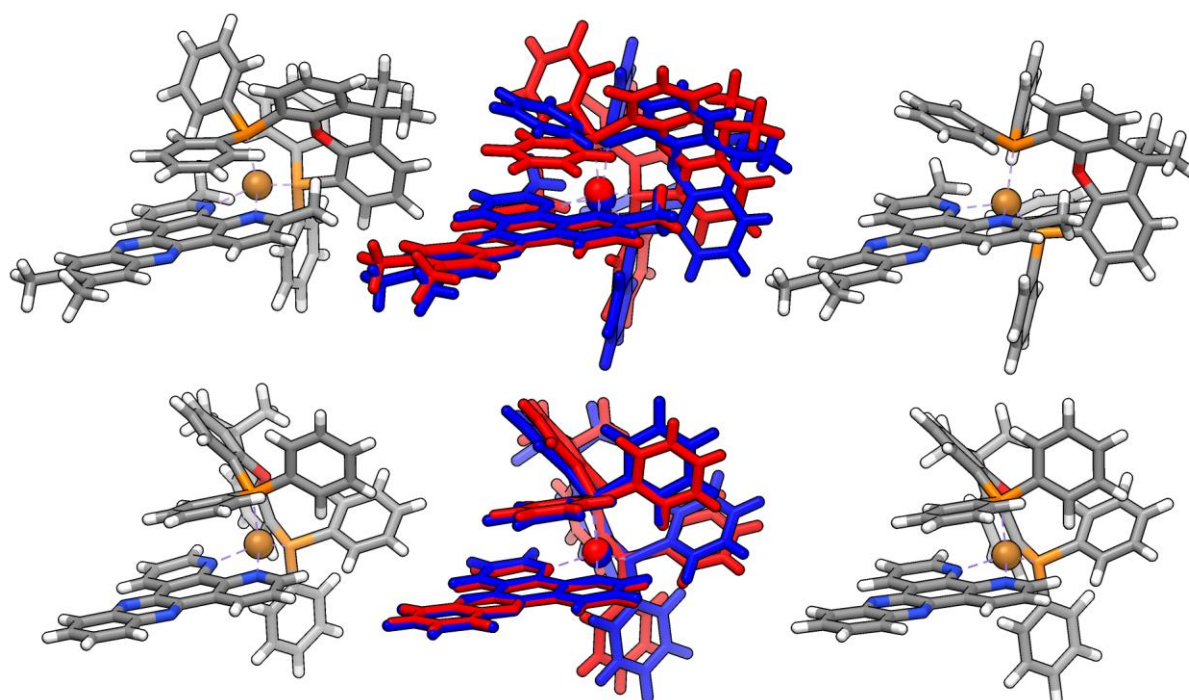


Figure S8. Comparison between the calculated geometries (left) and the X-ray structures (right) of **2** (top) and **1** (bottom). The overlapping of the simulated (in red) and experimental structures (in blue) is plotted in the middle.

Table S3. Selected crystallographic bond lengths (Å) for X-ray structure and the DFT-calculated geometry of **1** and **2**, as well as the mean bond lengths of Cu—N and Cu—P.

Compound	1		2	
	X-ray	DFT	X-ray	DFT
Cu-N1	2.097	2.109	2.099	2.132
Cu-N2	2.069	2.101	2.106	2.128
Mean	2.083	2.105	2.103	2.130
Cu-P1	2.286	2.312	2.283	2.320
Cu-P2	2.231	2.239	2.253	2.271
Mean	2.258	2.276	2.268	2.296

Table S4. Electronic transitions for **1**: Calculated vertical excitation energies (En.), wavelengths (λ), oscillator strengths (f) and eigenvalues of s^2 of the main excited states in the UV and visible range. The transitions are visualized by the accompanying shift of charge density from blue to red in combination with the originating MOs and their weights to the excited state.

ES Nr.	En. eV	λ nm	f	$\langle s^2 \rangle$	Wgt. %	from	to	Hole	Electron
1	2.40	516	0.0180	0.000	98	239	240		
3	2.87	432	0.1053	0.000	89	239	241		
10	3.41	364	0.0106	0.000	28 16 53	235 237 238	240 242 242		
11	3.42	363	0.0165	0.000	69 21	235 238	240 242		
13	3.63	342	0.2063	0.000	18 58 16	233 234 235	240 240 242		

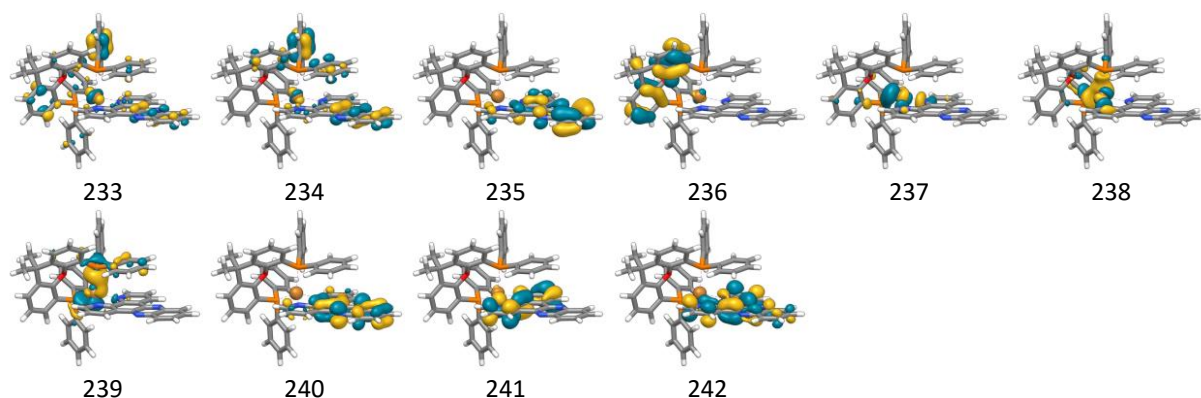
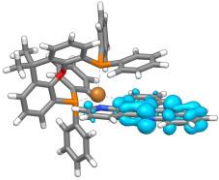
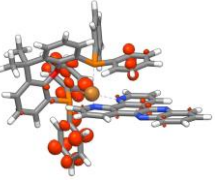
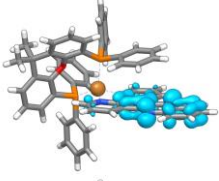
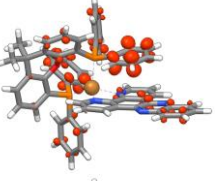
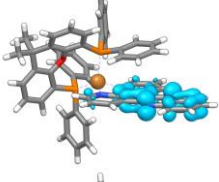
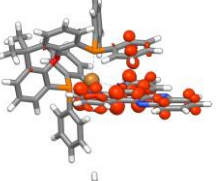
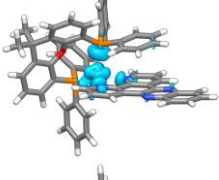
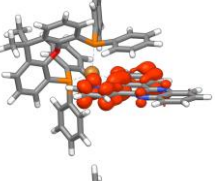
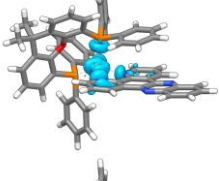
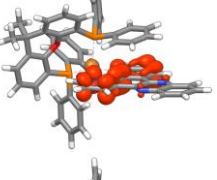
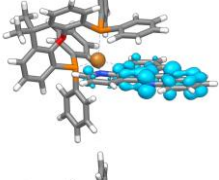
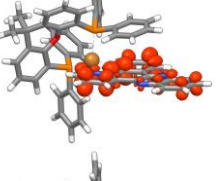
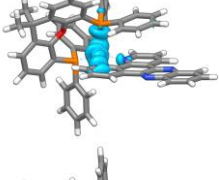
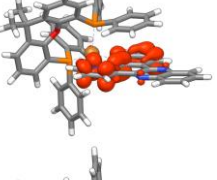
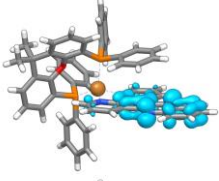
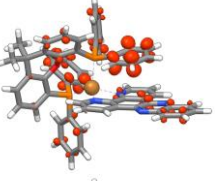
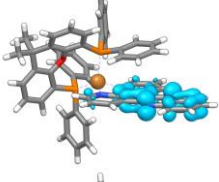
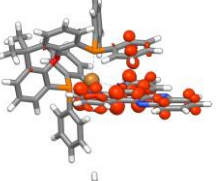
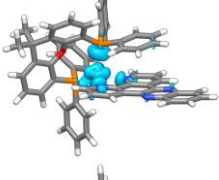
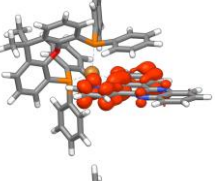
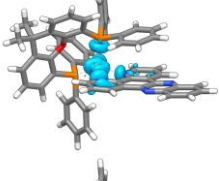
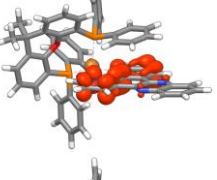
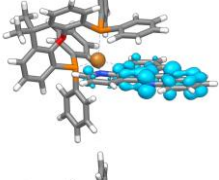
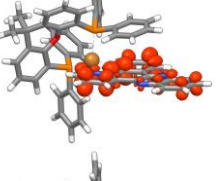
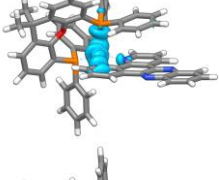
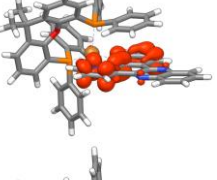
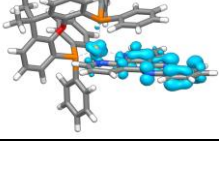
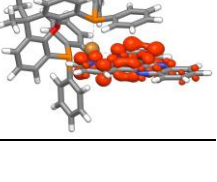


Table S5. Electronic transitions for the singly reduced state of **1**: Calculated vertical excitation energies (En.), wavelengths (λ), oscillator strengths (f) and eigenvalues of s^2 of the main excited states in the UV and visible range. The transitions are visualized by the accompanying shift of charge density from blue to red in combination with the originating MOs and their weights to the excited state.

ES Nr.	En. eV	λ nm	f	$\langle s^2 \rangle$	Wgt. %	from	to	Hole	Electron																																																																																																												
7	2.17	572	0.0495	0.770	76	240A	247A																																																																																																														
					13	240A	250A			9	2.27	547	0.0463	0.772	13	240A	247A			18	240A	248A	9	240A	249A	39	240A	250A	10	2.31	536	0.1052	0.785	10	240A	253A			19	240A	251A	38	240A	253A	21	3.08	403	0.0788	1.490	20	240A	254A			8	238A	241A	24	239A	241A	11	237B	241B	22	3.08	403	0.0398	1.971	32	239B	240B			34	238A	241A	9	237B	241B	23	3.13	396	0.0152	1.189	22	239B	240B			69	240A	258A	27	3.28	377	0.0209	0.848	34	238A	241A			17	237B	240B	20	237B	241B	13	239B	241B	28	3.37	368	0.0383	2.522	11
9	2.27	547	0.0463	0.772	13	240A	247A																																																																																																														
					18	240A	248A																																																																																																														
					9	240A	249A																																																																																																														
					39	240A	250A																																																																																																														
10	2.31	536	0.1052	0.785	10	240A	253A																																																																																																														
					19	240A	251A																																																																																																														
					38	240A	253A																																																																																																														
21	3.08	403	0.0788	1.490	20	240A	254A																																																																																																														
					8	238A	241A																																																																																																														
					24	239A	241A																																																																																																														
					11	237B	241B																																																																																																														
22	3.08	403	0.0398	1.971	32	239B	240B																																																																																																														
					34	238A	241A																																																																																																														
					9	237B	241B																																																																																																														
23	3.13	396	0.0152	1.189	22	239B	240B																																																																																																														
					69	240A	258A																																																																																																														
27	3.28	377	0.0209	0.848	34	238A	241A																																																																																																														
					17	237B	240B																																																																																																														
					20	237B	241B																																																																																																														
					13	239B	241B																																																																																																														
28	3.37	368	0.0383	2.522	11	237A	242A																																																																																																														
					44	238B	242B																																																																																																														

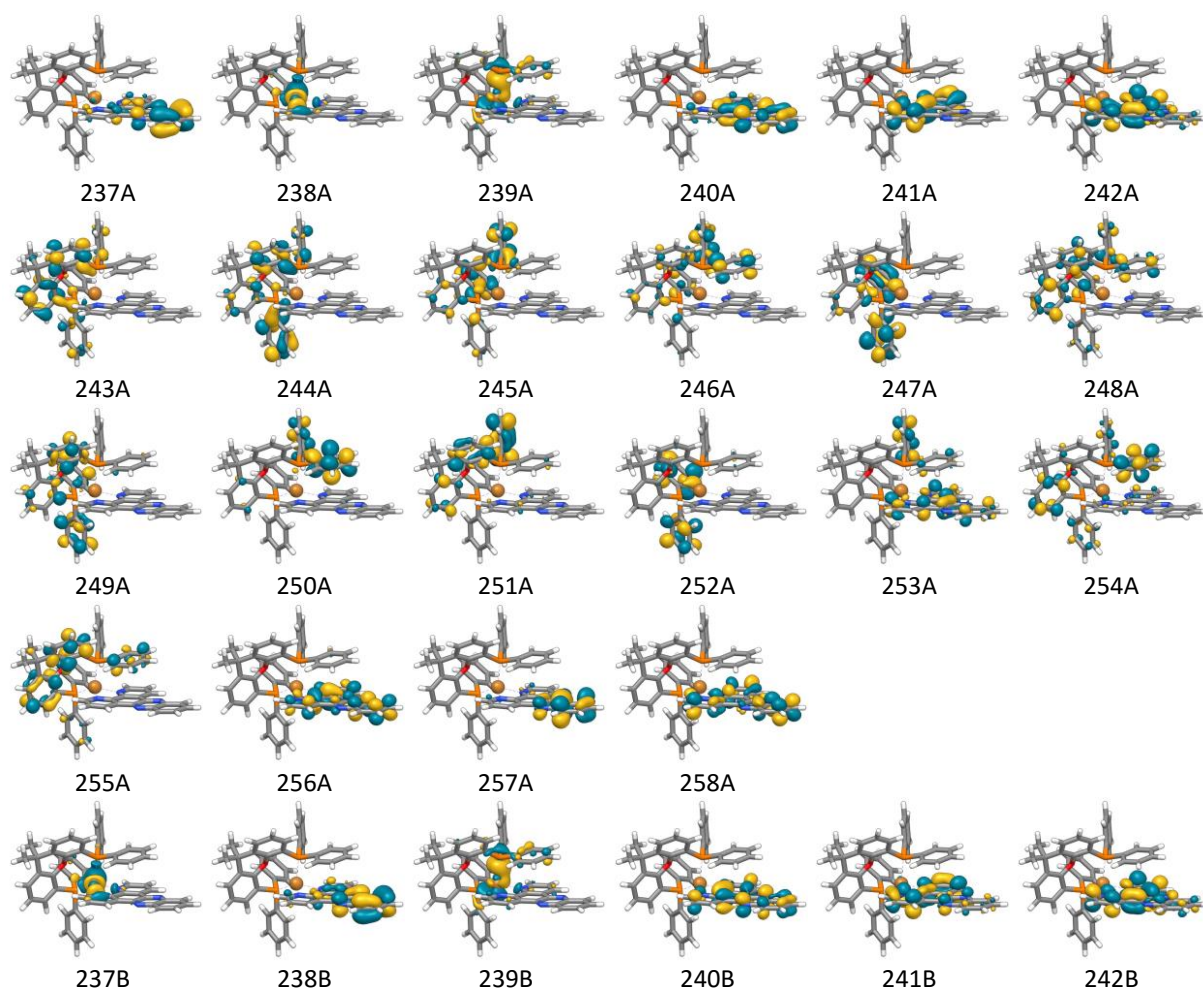


Table S6. Electronic transitions for **2**: Calculated vertical excitation energies (E_n), wavelengths (λ), oscillator strengths (f) and eigenvalues of s^2 of the main excited states in the UV and visible range. The transitions are visualized by the accompanying shift of charge density from blue to red in combination with the originating MOs and their weights to the excited state.

ES Nr.	E_n eV	λ nm	f	$\langle s^2 \rangle$	Wgt. %	from	to	Hole	Electron
1	2.58	481	0.0455	0.000	97	255	256		
2	2.96	419	0.0572	0.000	85	255	257		
8	3.32	373	0.0152	0.000	77 13	251 252	256 256		
9	3.42	362	0.0209	0.000	67 14	253 254	257 257		
10	3.45	359	0.0128	0.000	13 78	251 252	256 256		
11	3.53	351	0.3007	0.000	79 13	250 251	256 258		

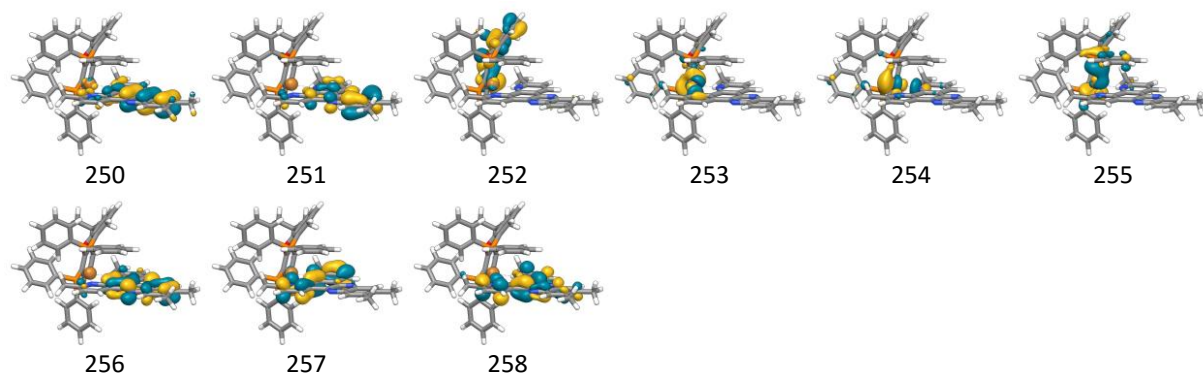
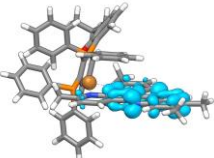
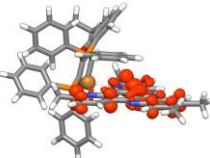
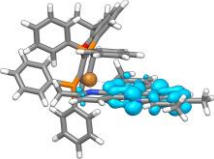
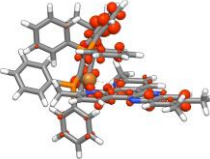
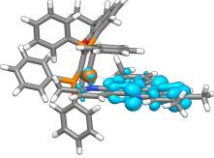
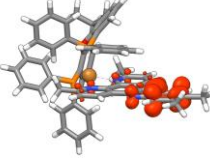
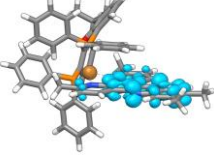
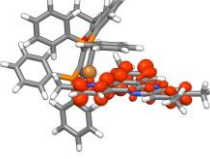
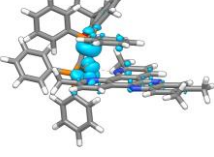
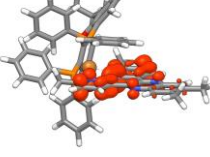
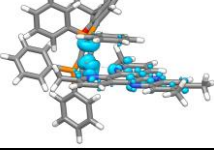
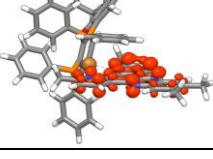
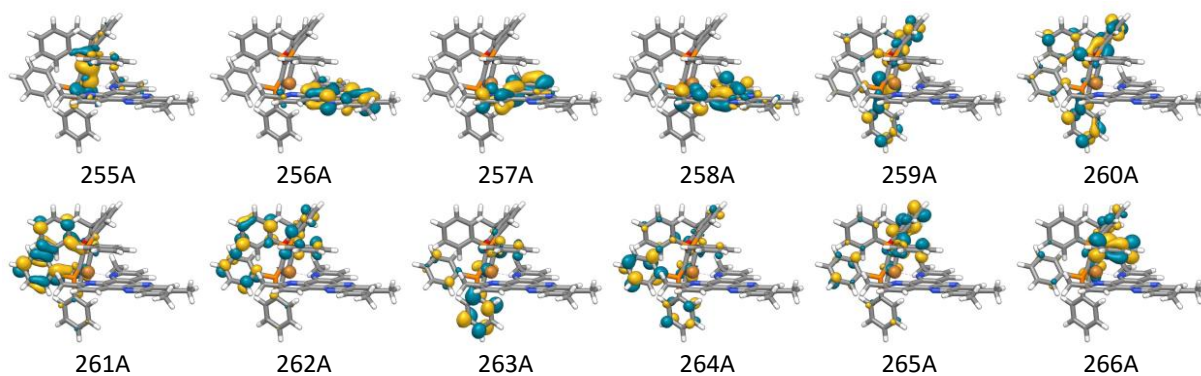


Table S7. Electronic transitions for the singly reduced state of **2**: Calculated vertical excitation energies (En.), wavelengths (λ), oscillator strengths (f) and eigenvalues of s^2 of the main excited states in the UV and visible range. The transitions are visualized by the accompanying shift of charge density from blue to red in combination with the originating MOs and their weights to the excited state.

ES Nr.	En. eV	λ nm	f	$\langle s^2 \rangle$	Wgt. %	from	to	Hole	Electron
11	2.27	546	0.1674	0.786	21	256A	269A		
					9	256A	270A		
					51	256A	271A		
13	2.37	523	0.0103	0.778	12	256A	266A		
					24	256A	268A		
					23	256A	269A		
					10	256A	270A		
					23	256A	272A		
18	2.90	427	0.0124	0.988	80	256A	273A		
22	3.07	404	0.0309	1.338	63	256A	274A		
23	3.15	394	0.1754	0.811	30	255A	257A		
					60	254B	256B		
25	3.30	376	0.0346	1.216	14	255A	257A		
					9	254B	256B		
					39	254B	257B		



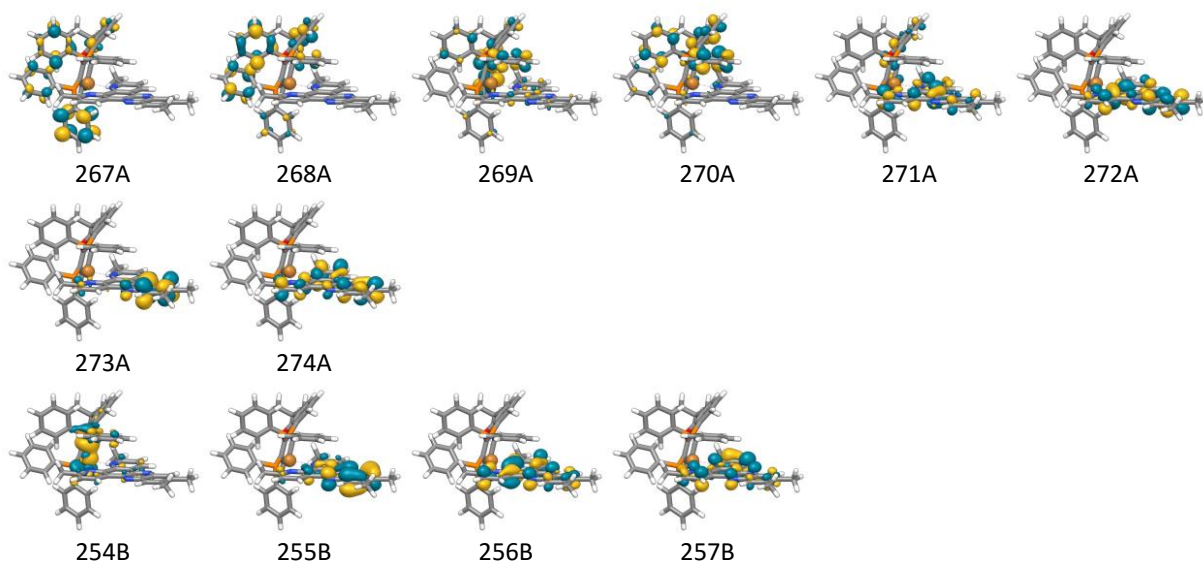
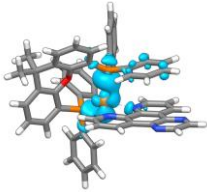
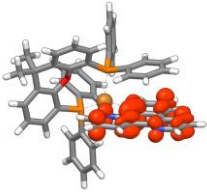
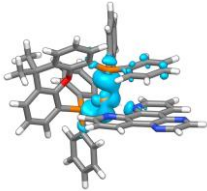
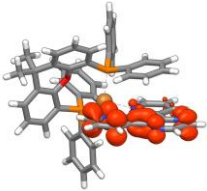
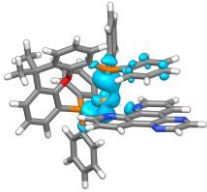
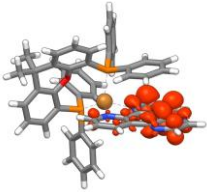
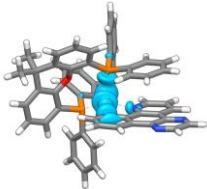
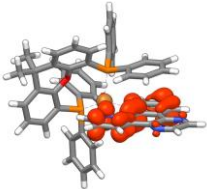
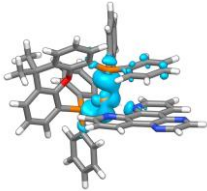
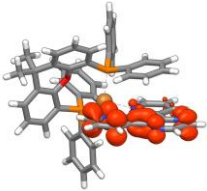
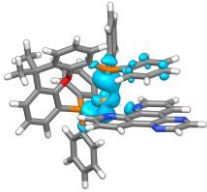
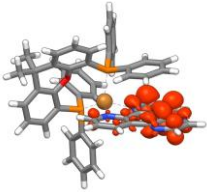
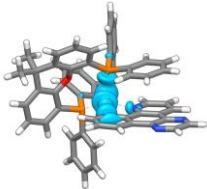
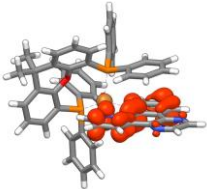
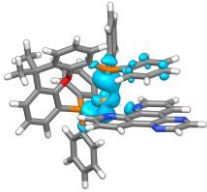
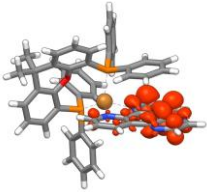
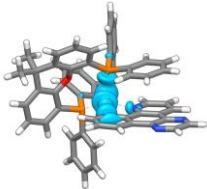
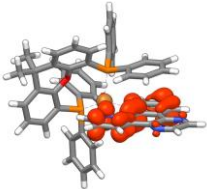
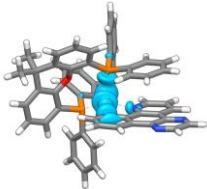
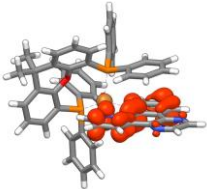


Table S8. Electronic transitions for **3**: Calculated vertical excitation energies (En.), wavelengths (λ), oscillator strengths (f) and eigenvalues of s^2 of the main excited states in the UV and visible range. The transitions are visualized by the accompanying shift of charge density from blue to red in combination with the originating MOs and their weights to the excited state.

ES Nr.	En. eV	λ nm	f	$\langle s^2 \rangle$	Wgt. %	from	to	Hole	Electron																																						
1	2.76	450	0.0581	0.000	80	226	227																																								
					17	226	228			2	2.93	423	0.0246	0.000	15	226	227			72	226	228	3	2.94	422	0.0139	0.000	89	226	229						4	3.02	410	0.0198	0.000	11	224	227			15	224
2	2.93	423	0.0246	0.000	15	226	227																																								
					72	226	228			3	2.94	422	0.0139	0.000	89	226	229						4	3.02	410	0.0198	0.000	11	224	227			15	224	228						23	225	227			36	225
3	2.94	422	0.0139	0.000	89	226	229																																								
										4	3.02	410	0.0198	0.000	11	224	227			15	224	228						23	225	227			36	225	228												
4	3.02	410	0.0198	0.000	11	224	227																																								
					15	224	228																																								
					23	225	227																																								
					36	225	228																																								

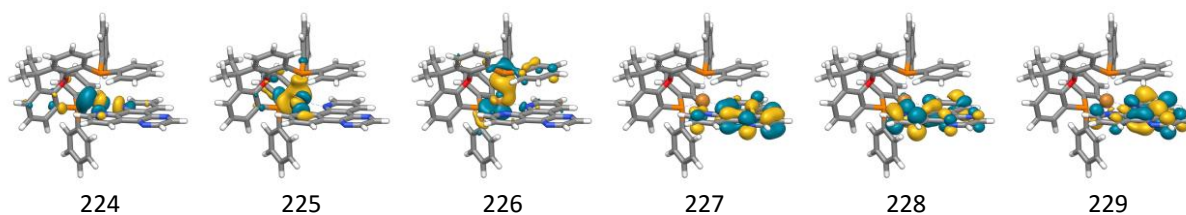
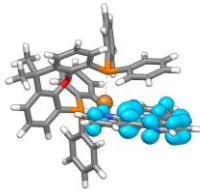
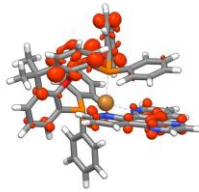
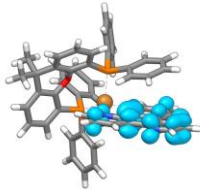
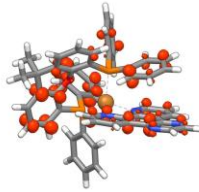
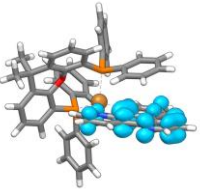
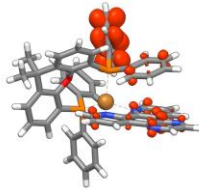
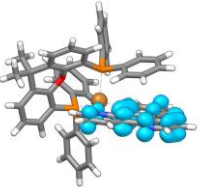
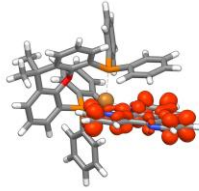
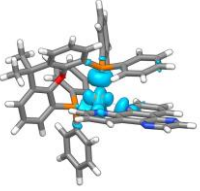
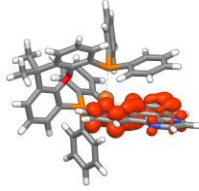
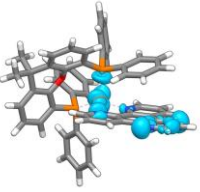
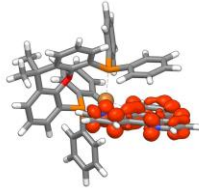
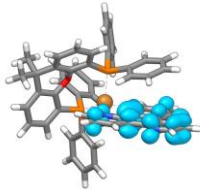
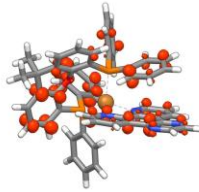
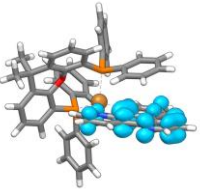
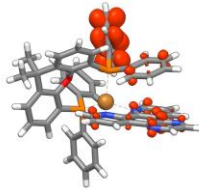
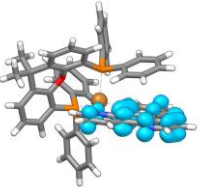
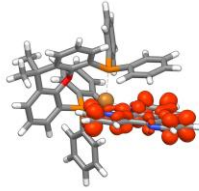
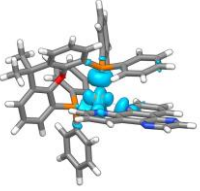
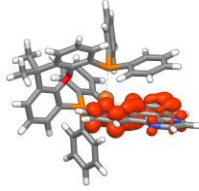
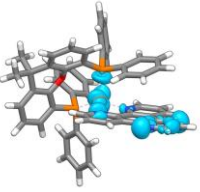
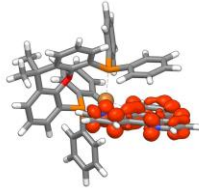
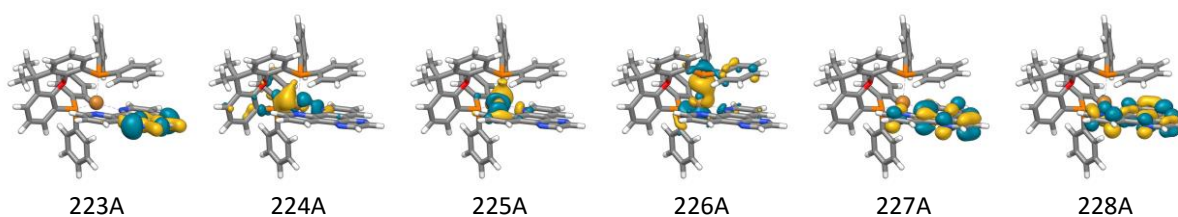


Table S9. Electronic transitions for the singly reduced state of **3**: Calculated vertical excitation energies (En.), wavelengths (λ), oscillator strengths (f) and eigenvalues of s^2 of the main excited states in the UV and visible range. The transitions are visualized by the accompanying shift of charge density from blue to red in combination with the originating MOs and their weights to the excited state.

ES Nr.	En. eV	λ nm	f	$\langle s^2 \rangle$	Wgt. %	from	to	Hole	Electron																																																																											
11	2.06	602	0.0209	0.771	66 20	227A	238A																																																																													
						227A	242A			12	2.12	585	0.0138	0.771	25 29 25	227A	239A			227A	240A	227A	242A	14	2.17	570	0.0123	0.771	28 25 17 22	227A	238A			227A	240A	227A	241A	227A	242A	17	2.92	425	0.0418	0.900	20 63	227A	244A			227A	245A	21	3.21	386	0.0540	0.845	11 23 50	225A	228A			226A	228A	226B	227B	24	3.30	376	0.0235	1.148	11 20 18 26 10	223A	228A			225A	228A	222B	229B	225B	227B			
12	2.12	585	0.0138	0.771	25 29 25	227A	239A																																																																													
						227A	240A																																																																													
						227A	242A																																																																													
14	2.17	570	0.0123	0.771	28 25 17 22	227A	238A																																																																													
						227A	240A																																																																													
						227A	241A																																																																													
						227A	242A																																																																													
17	2.92	425	0.0418	0.900	20 63	227A	244A																																																																													
						227A	245A																																																																													
21	3.21	386	0.0540	0.845	11 23 50	225A	228A																																																																													
						226A	228A																																																																													
						226B	227B																																																																													
24	3.30	376	0.0235	1.148	11 20 18 26 10	223A	228A																																																																													
						225A	228A																																																																													
						222B	229B																																																																													
						225B	227B																																																																													
						10	226B	227B																																																																												



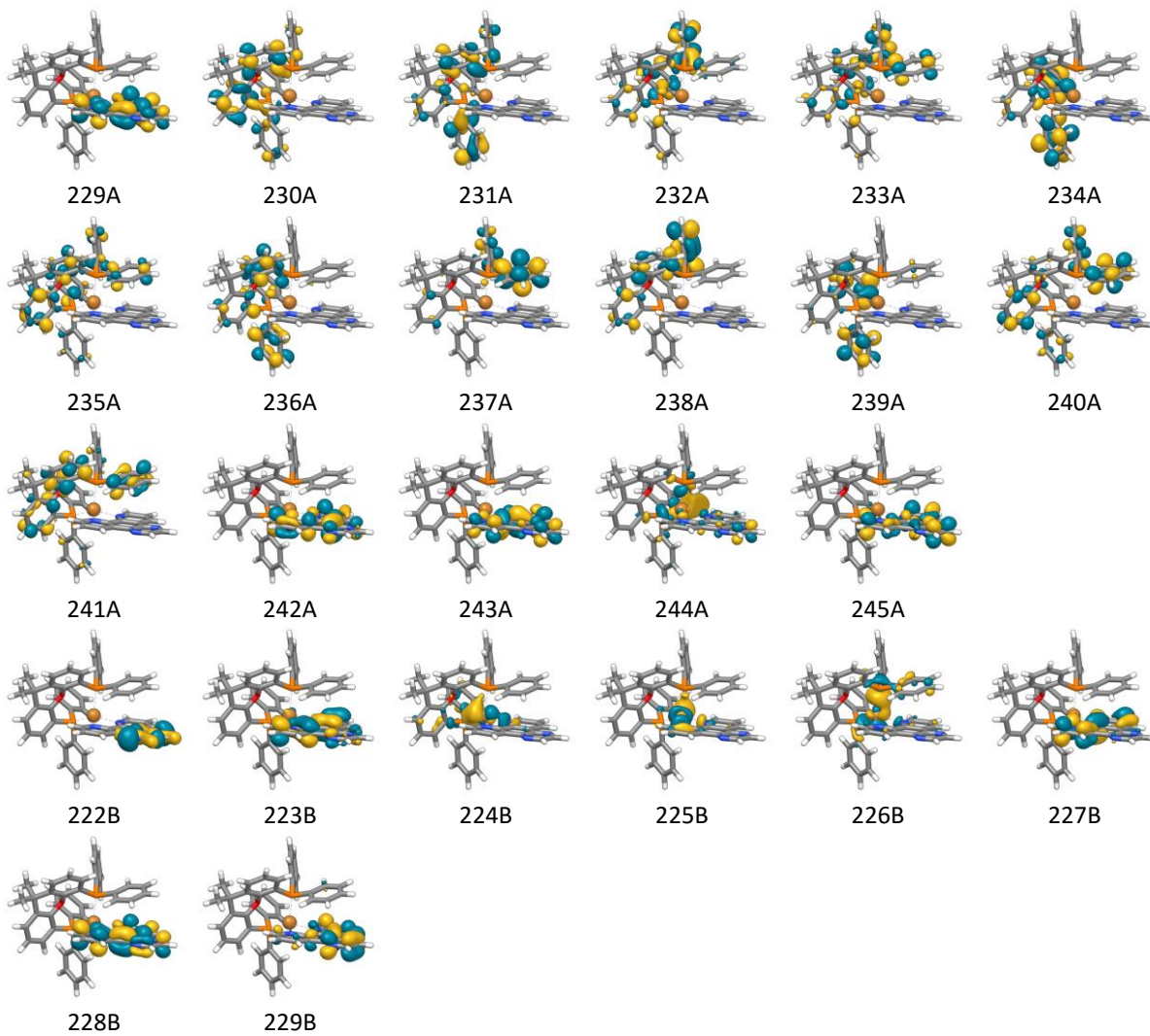
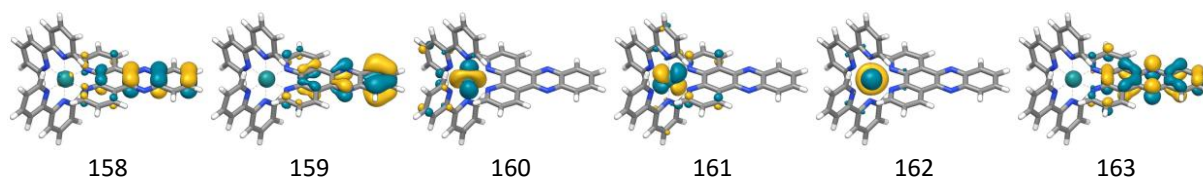


Table S10. Electronic transitions for **5**: Calculated vertical excitation energies (En.), wavelengths (λ), oscillator strengths (f) and eigenvalues of s^2 of the main excited states in the UV and visible range. The transitions are visualized by the accompanying shift of charge density from blue to red in combination with the originating MOs and their weights to the excited state.

ES Nr.	En. eV	λ nm	f	$\langle s^2 \rangle$	Wgt. %	from	to	Hole	Electron																																																																																																				
4	2.68	463	0.0876	0.000	88	161	163																																																																																																						
					9	161	164			9	2.90	428	0.0452	0.000	20	160	163			63	160	164	10	2.94	422	0.0898	0.000	20	160	165			37	160	166	21	161	165	11	161	166	11	2.97	417	0.1307	0.000	26	160	165			14	160	166	20	161	164	10	161	165	12	3.04	408	0.0290	0.000	19	161	166			12	160	165	71	162	167	16	3.30	375	0.0792	0.000	58	160	167			12	161	166	9	162	167	17	3.39	366	0.0349	0.000	91	159	163			19	3.68	337	0.1391	0.000	65	158
9	2.90	428	0.0452	0.000	20	160	163																																																																																																						
					63	160	164			10	2.94	422	0.0898	0.000	20	160	165			37	160	166						21	161	165			11	161	166	11	2.97	417	0.1307	0.000	26						160	165					14	160	166	20	161	164	10	161						165	12	3.04			408	0.0290	0.000	19	161	166								12			160	165	71	162	167	16	3.30	375	0.0792	0.000	58	160	167			12	161	166	9	162	167	17	3.39
10	2.94	422	0.0898	0.000	20	160	165																																																																																																						
					37	160	166																																																																																																						
					21	161	165																																																																																																						
					11	161	166																																																																																																						
11	2.97	417	0.1307	0.000	26	160	165																																																																																																						
					14	160	166																																																																																																						
					20	161	164																																																																																																						
					10	161	165																																																																																																						
12	3.04	408	0.0290	0.000	19	161	166																																																																																																						
					12	160	165																																																																																																						
					71	162	167																																																																																																						
16	3.30	375	0.0792	0.000	58	160	167																																																																																																						
					12	161	166																																																																																																						
					9	162	167																																																																																																						
17	3.39	366	0.0349	0.000	91	159	163																																																																																																						
19	3.68	337	0.1391	0.000	65	158	163																																																																																																						
					27	159	167																																																																																																						



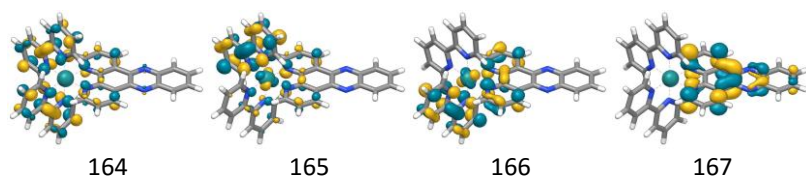
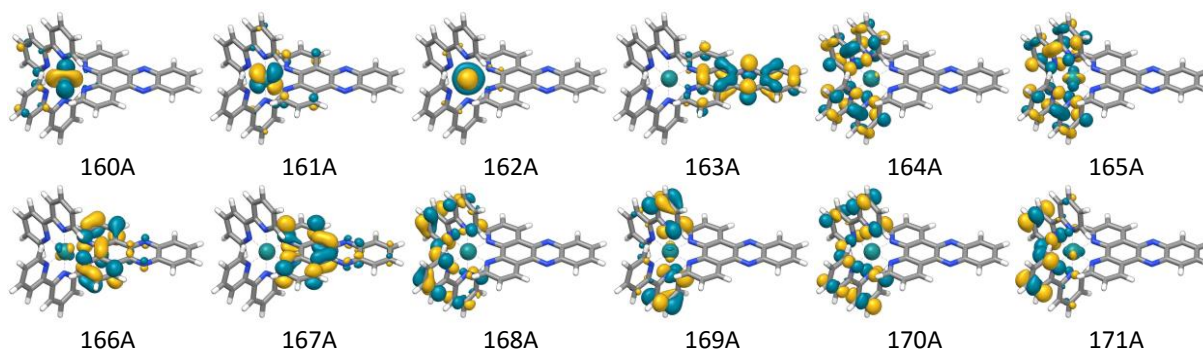


Table S11. Electronic transitions for the singly reduced state of **5**: Calculated vertical excitation energies (En.), wavelengths (λ), oscillator strengths (f) and eigenvalues of s^2 of the main excited states in the UV and visible range. The transitions are visualized by the accompanying shift of charge density from blue to red in combination with the originating MOs and their weights to the excited state.

ES Nr.	En. eV	λ nm	f	$\langle s^2 \rangle$	Wgt. %	from	to	Hole	Electron
10	2.29	542	0.1778	0.807	95	163A	172A		
22	2.77	447	0.1253	0.886	29	160A	164A		
					13	161A	165A		
					26	159B	163B		
					14	160B	164B		
27	2.91	426	0.1263	0.772	36	160A	165A		
					35	159B	164B		
36	3.15	393	0.0146	2.074	16	163A	179A		
					12	161B	165B		
					9	162B	166B		
38	3.16	392	0.0192	1.961	8	163A	176A		
					20	163A	179A		
40	3.19	389	0.0785	0.888	24	161A	166A		
					51	160B	165B		



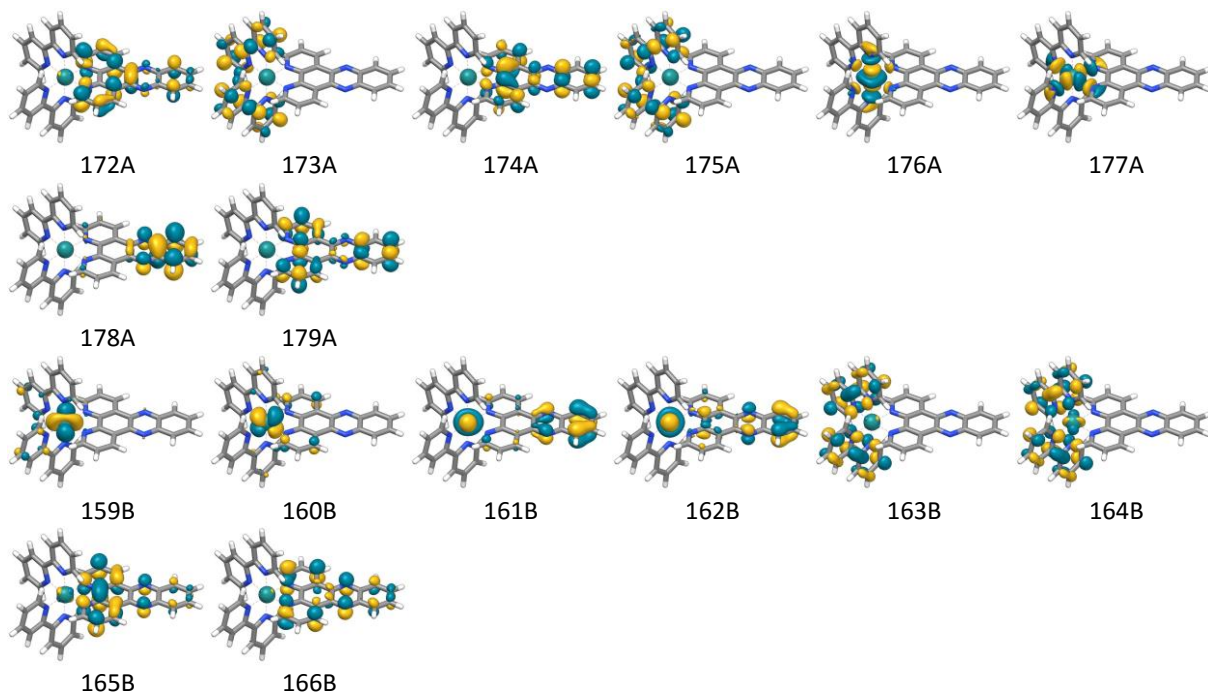


Table S12. Electronic transitions for **6**: Calculated vertical excitation energies (En.), wavelengths (λ), oscillator strengths (f) and eigenvalues of s^2 of the main excited states in the UV and visible range. The transitions are visualized by the accompanying shift of charge density from blue to red in combination with the originating MOs and their weights to the excited state.

ES Nr.	En. eV	λ nm	f	$\langle s^2 \rangle$	Wgt. %	from	to	Hole	Electron																																																																							
5	2.79	445	0.0501	0.000	76	148	150																																																																									
					19	148	151			7	2.87	431	0.0641	0.000	22	147	152			14	148	150	46	148	151	14	149	154	8	2.93	423	0.1301	0.000	51	147	151			37	148	152	9	2.95	420	0.0716	0.000	22	147	152			70	149	154	12	3.15	393	0.0139	0.000	81	147	154			13	3.17	391	0.0249	0.000	94	148	154			15	3.30	374	0.0427	0.000	10
7	2.87	431	0.0641	0.000	22	147	152																																																																									
					14	148	150																																																																									
					46	148	151																																																																									
					14	149	154																																																																									
8	2.93	423	0.1301	0.000	51	147	151																																																																									
					37	148	152			9	2.95	420	0.0716	0.000	22	147	152			70	149	154	12	3.15	393	0.0139	0.000	81	147	154			13	3.17	391	0.0249	0.000	94	148	154			15	3.30	374	0.0427	0.000	10	147	152			73	148	153																									
9	2.95	420	0.0716	0.000	22	147	152																																																																									
					70	149	154																																																																									
12	3.15	393	0.0139	0.000	81	147	154																																																																									
13	3.17	391	0.0249	0.000	94	148	154																																																																									
15	3.30	374	0.0427	0.000	10	147	152																																																																									
					73	148	153																																																																									

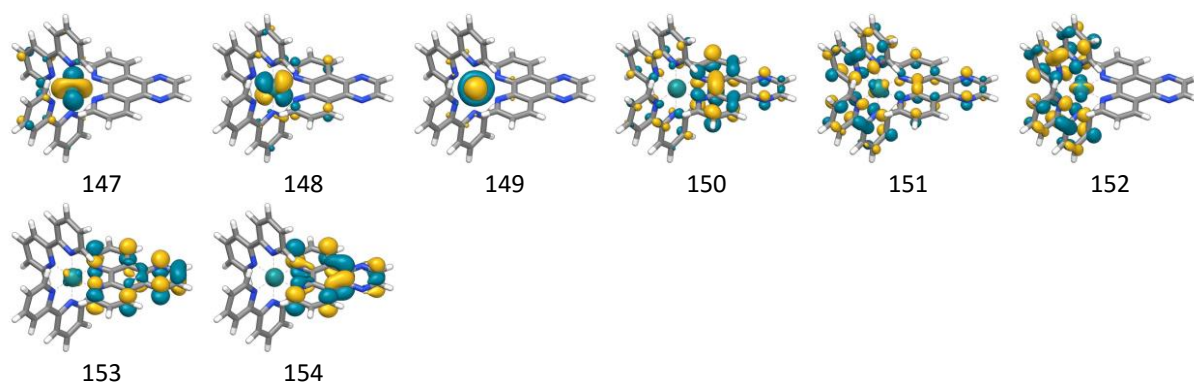
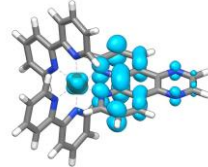
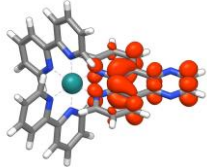
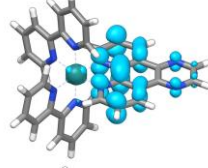
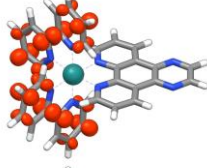
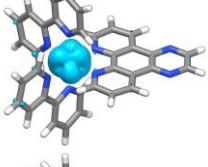
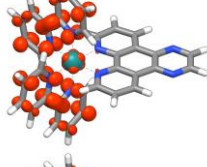
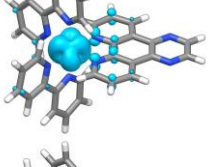

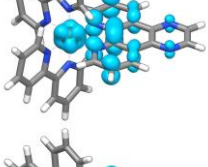
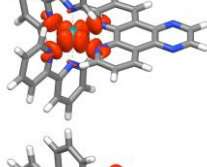

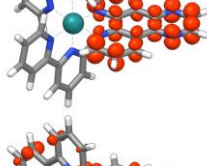

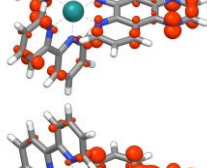
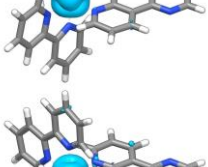
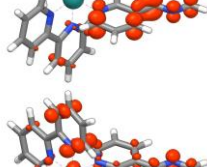
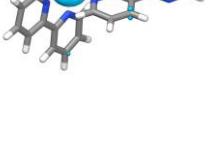
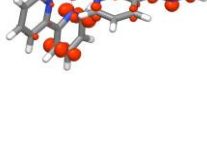
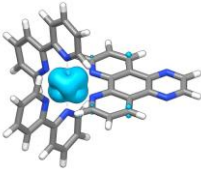
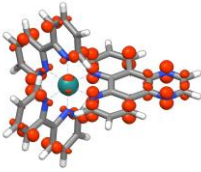
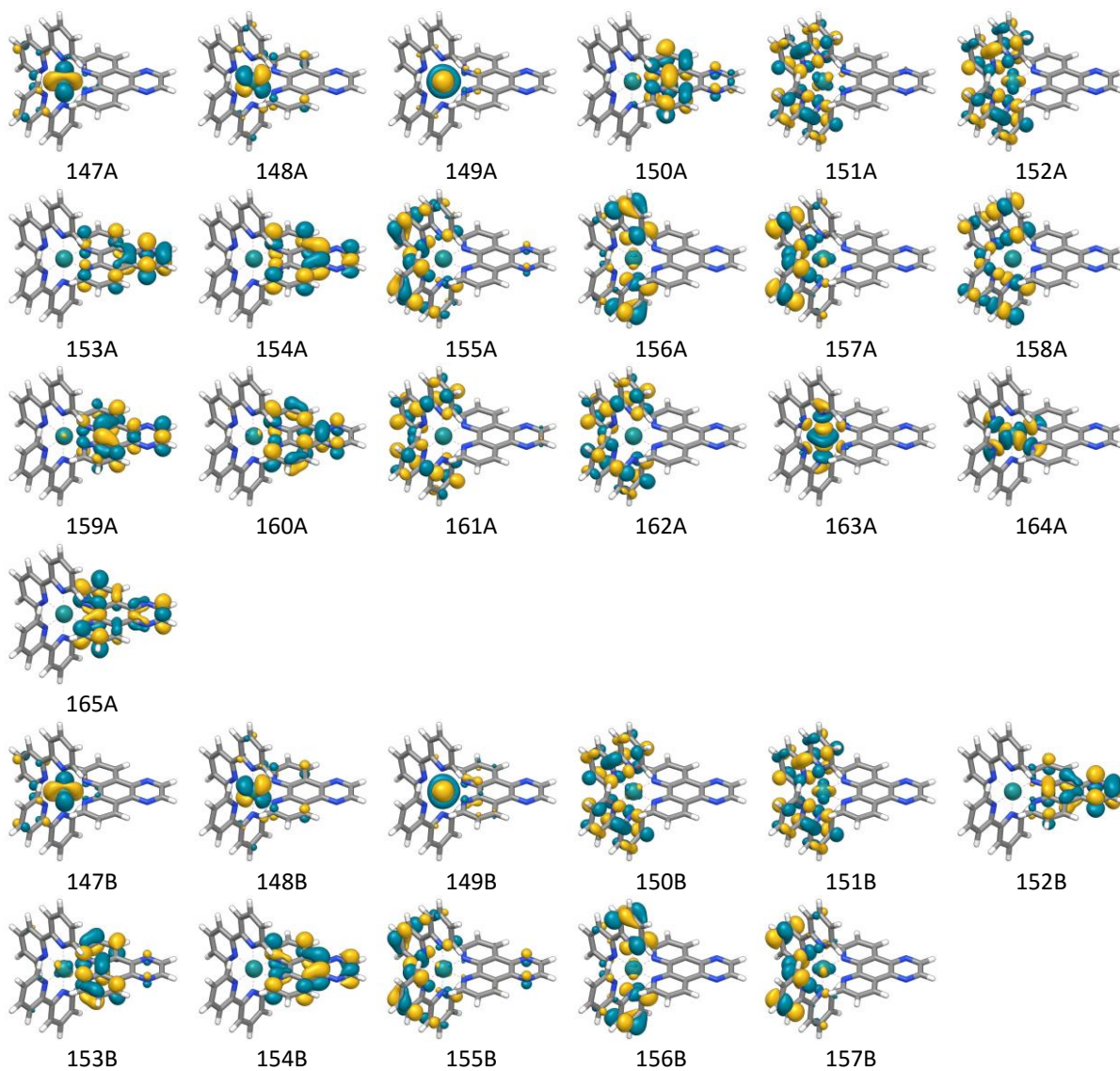


Table S13. Electronic transitions for the singly reduced state of **6**: Calculated vertical excitation energies (En.), wavelengths (λ), oscillator strengths (f) and eigenvalues of s^2 of the main excited states in the UV and visible range. The transitions are visualized by the accompanying shift of charge density from blue to red in combination with the originating MOs and their weights to the excited state.

ES Nr.	En. eV	λ nm	f	$\langle s^2 \rangle$	Wgt. %	from	to	Hole	Electron
13	2.25	551	0.0298	0.790	87	150A	159A		
21	2.62	472	0.0168	0.774	92	150A	161A		
22	2.68	462	0.1413	0.773	24	147A	151A		
					17	148A	152A		
					34	147B	150B		
					19	148B	151B		
25	2.82	440	0.0508	0.808	24	147A	152A		
					17	150A	164A		
					31	147B	151B		
					9	148B	150B		
26	2.85	435	0.0177	0.819	79	150A	164A		
28	2.99	415	0.0202	1.715	18	149A	153A		
					42	150A	165A		
					15	149B	152B		
32	3.12	398	0.0119	1.527	9	149A	153A		
					27	149B	152B		
					24	149B	153B		
					13	149B	155B		
41	3.25	381	0.0177	1.207	35	149A	154A		
					13	148B	152B		
					22	149B	154B		
42	3.29	377	0.0181	2.327	14	148B	152B		
					15	149B	154B		
					16	149B	156B		
					9	149B	157B		

ES Nr.	En. eV	λ nm	f	$\langle s^2 \rangle$	Wgt. %	from	to	Hole	Electron
45	3.34	371	0.0259	1.432	18 12 24	148A 149A 148B	153A 156A 153B		



6 UV-Vis-SEC on the redox of complexes 1–4

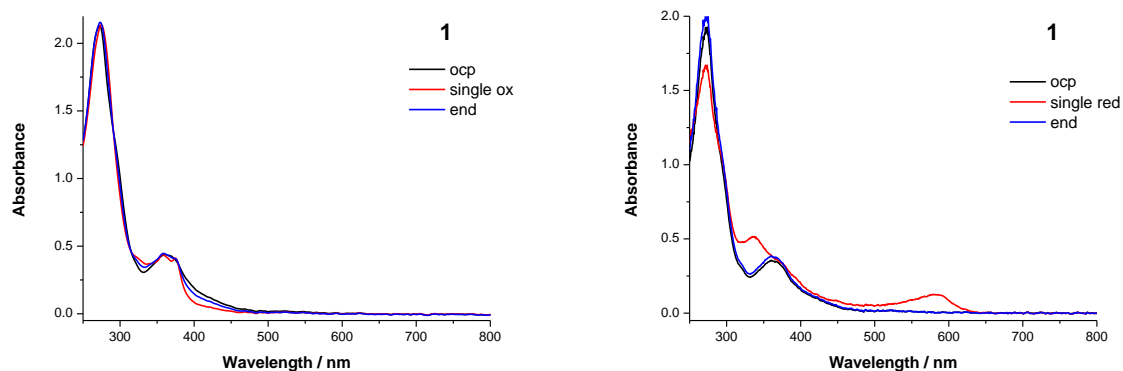


Figure S9. UV-Vis absorption spectroelectrochemistry of complex **1** upon electrochemical oxidation (left) and reduction (right) in ACN/ 0.1 M TBAPF₆ solutions. The “open circuit potential” spectra (ocp) are collected without external potential and the “end” spectra are recorded 5 minutes after the SEC measurement to check the recovery.

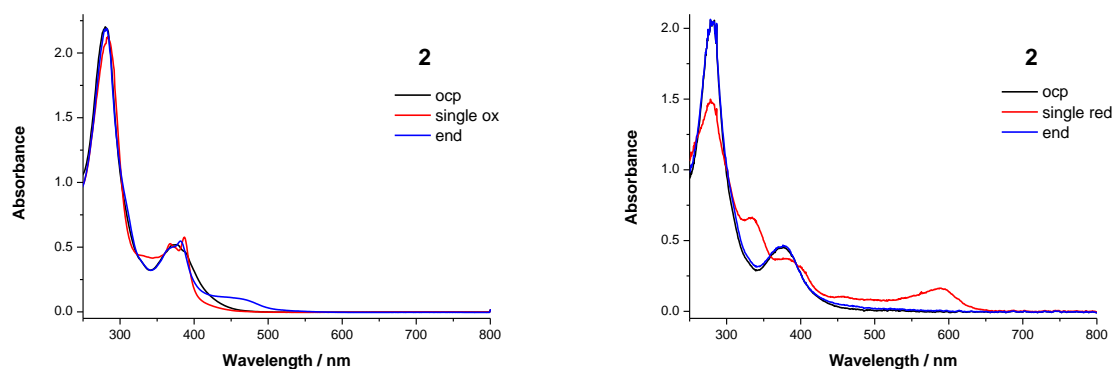


Figure S10. UV-Vis absorption spectroelectrochemistry of complex **2** upon reduction (left) and oxidation (right) in ACN/ 0.1 M TBAPF₆ solutions. The “ocp” spectra are collected without external potential and the “end” spectra are recorded 5 minutes after the SEC measurement to check the recovery.

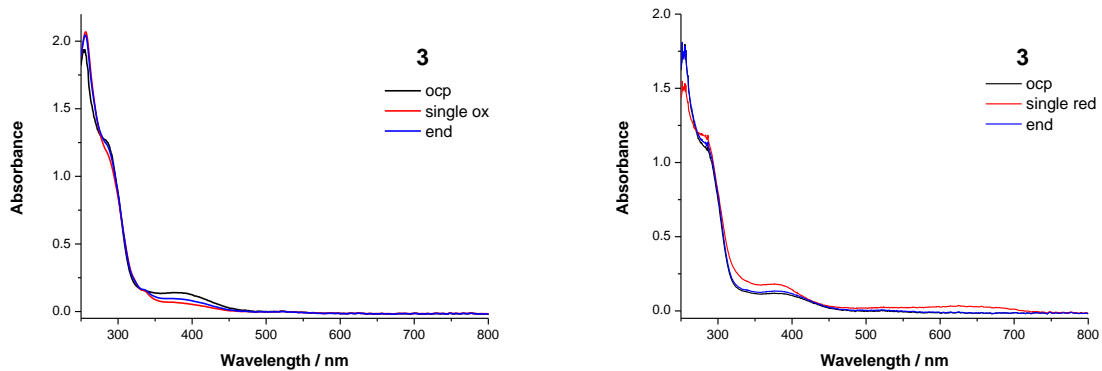


Figure S11. UV-Vis absorption spectroelectrochemistry of complex **3** upon reduction (left) and oxidation (right) in ACN/ 0.1 M TBAPF₆ solutions. The “ocp” spectra are collected without external potential and the “end” spectra are recorded 5 minutes after the SEC measurement to check the recovery.

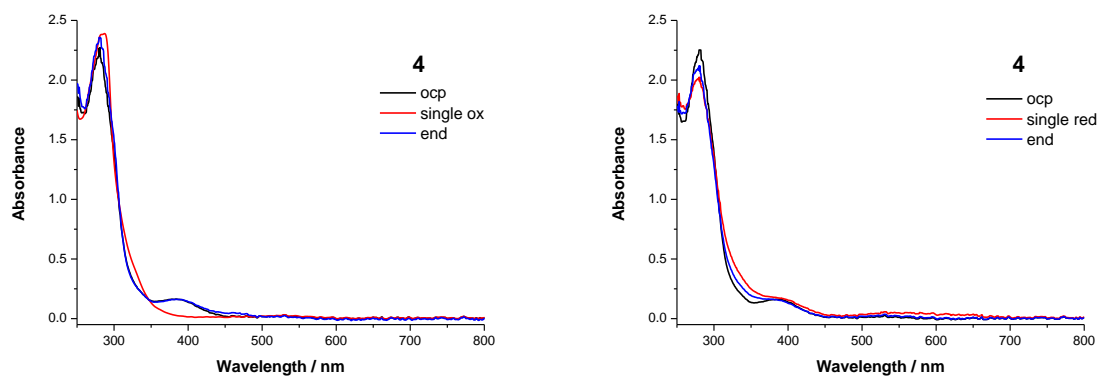


Figure S12. UV-Vis absorption spectroelectrochemistry of complex **4** upon reduction (left) and oxidation (right) in ACN/ 0.1 M TBAPF₆ solutions. The “ocp” spectra are collected without external potential and the “end” spectra are recorded 5 minutes after the SEC measurement to check the recovery.

7 RR data of complexes 1–7

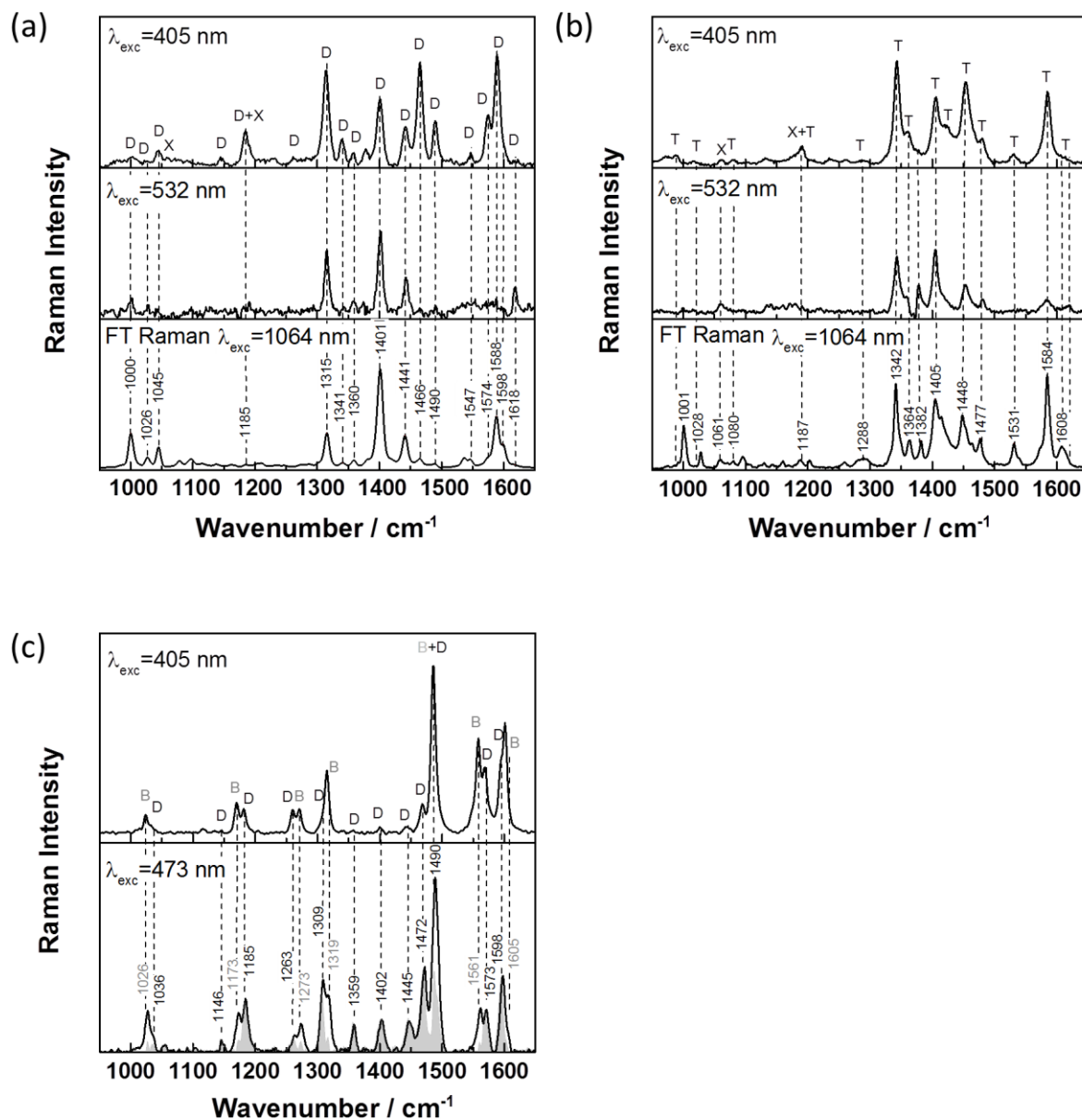


Figure S13. Resonance Raman spectra of complex **1** (a), **2** (b) and **5** (c) in ACN. Distinct excitation wavelength is specified in the panel. Characteristic bands are indicated with symbols for dppz (“D”), xant (“X”), tmdppz (“T”), bpy (“B”) ligands. Only the RR modes in associated with the excited state transitions are enhanced. Nonresonance FT-Raman spectra of **1** and **2** in solid state are depicted in the lower panel for reference. The shadows in (c) illustrate the dppz contribution in **5** (subtracted by RR of $[\text{Ru}(\text{bpy})_3]^{2+}$).

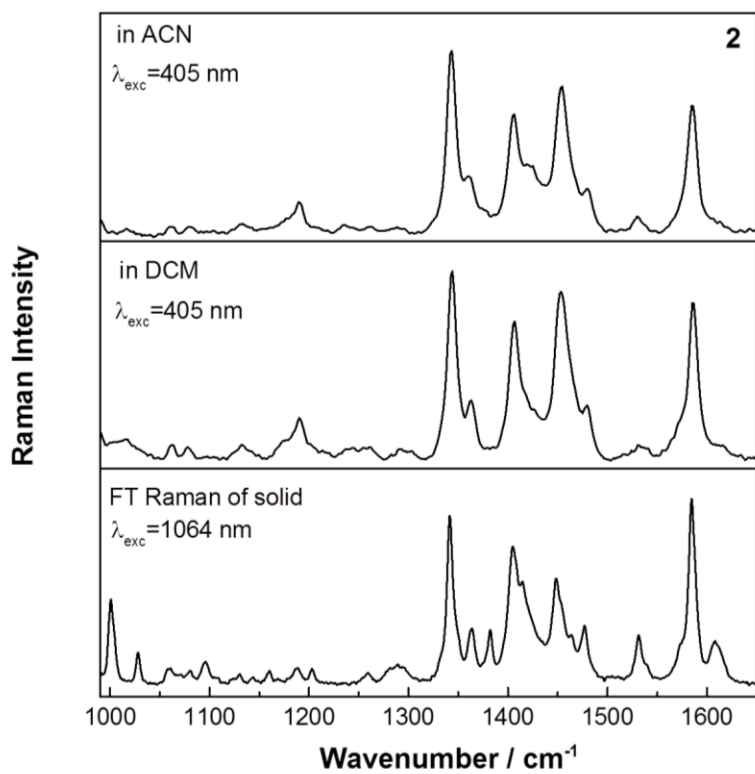


Figure S14. RR spectrum of complex **2** in ACN (upper panel) and in DCM (middle panel). Nonresonant FT-Raman spectra of the solid state sample is depicted in the last panel.

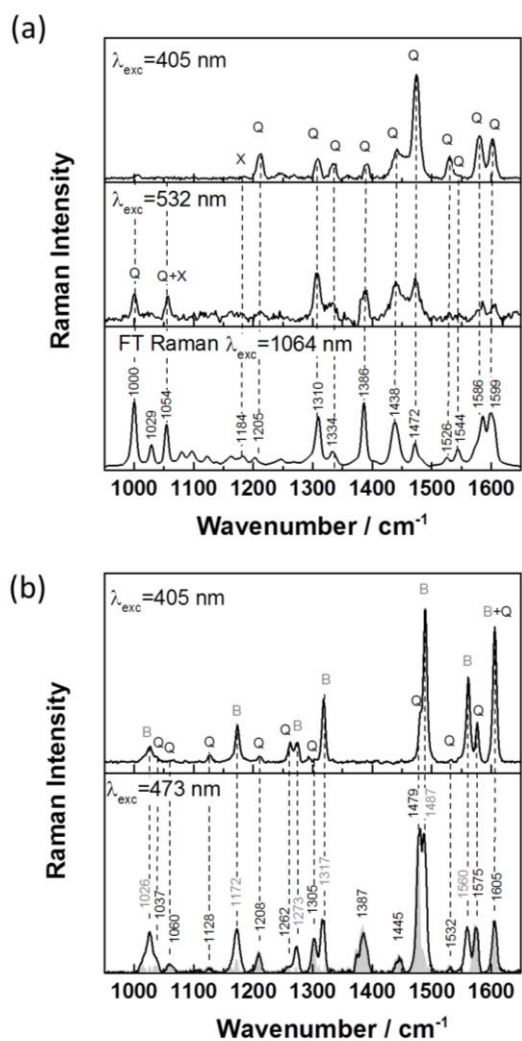


Figure S15. Resonance Raman spectra of complex **3** (a) and **6** (b) in ACN. Distinct excitation wavelength is specified in the panel. Characteristic bands are indicated with symbols for dpq (“Q”), xant (“X”) and bpy (“B”) ligands. Only the RR modes in associated with the excited state transitions are enhanced. Nonresonance FT-Raman spectrum of **3** in solid state is depicted in the lower panel for reference. The shadows in (b) illustrate the dpq contribution in **6** (subtracted by RR of [Ru(bpy)₃]²⁺).

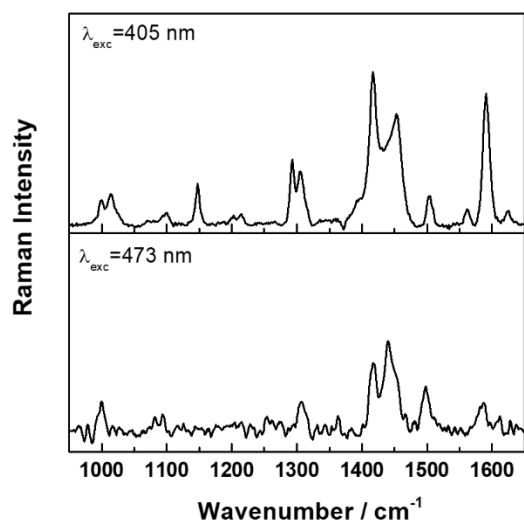


Figure S16. RR spectra of Cu(I) complex **4** in ACN at 405 and 473 nm excitation. All the strong bands (*i.e.* at 1589, 1560, 1502, 1446, 1420, 1303, 1293, 1146, 1017 and 1000 cm^{-1}) were assigned to the dmp ligands.

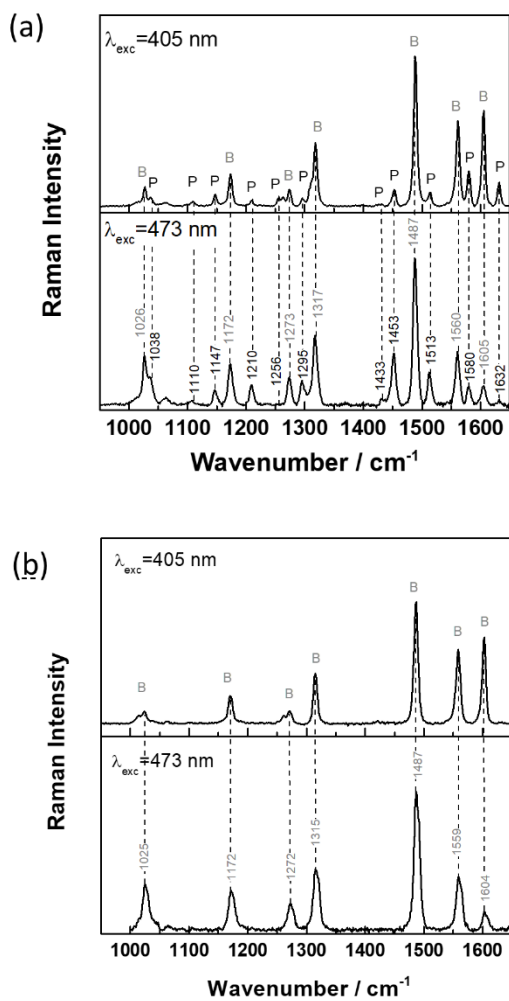


Figure S17. Resonance Raman spectra of complex **7** (a) and $[\text{Ru}(\text{bpy})_3]^{2+}$ (b) in ACN. Distinct excitation wavelength is specified in the panel. Characteristic bands are indicated with symbols for phen (“P”) and bpy (“B”) ligands.

Table S14. Wavenumber positions (in cm^{-1}) of the Raman bands of complexes **1**, **2** and **5**. The Raman bands are grouped into (tm)dppz and xant ligands for **1** and **2**, or dppz and bpy for **5**. In particular, dppz ligand can be considered to be constituted by 1,10-phenanthroline (phen) and phenazine (phz) fragments.

	1		2			5	Assignm ent
FT Raman	RR at 405 nm	RR at 532 nm	FT Raman	RR at 405 nm	RR at 532 nm	RR at 405/473 nm	
1618	1618	1618	1608	1610	1620		phz
						1605	bpy
1598						1597	phen
1588	1589		1584	1584	1584		phen
1574	1575		1574			1571	phen
						1560	bpy
1547							dppz
1536			1531	1531			phz
1490	1490		1477	1479	1480	1490	dppz
						1487	bpy
1466	1465		1448	1454	1453	1470	dppz
1441	1442	1442				1445	phen
			1415				dppz
1401	1401	1401	1405	1405	1405	1401	phz
			1382		1380		dppz
1360						1358	dppz
1341	1340		1364	1362			dppz
						1319	bpy
1315	1315	1315	1342	1344	1342	1308	phen
				1289			phen
						1272	bpy
				1260		1262	phen
1240				1239			dppz
1207			1203				phz
1185	1185		1189	1191		1183	phen+xant
	1146			1132		1173	bpy
1097			1097			1146	phz
1080	1075		1080	1081			xant
1045			1061	1062	1060		xant
1027	1046		1028			1034	dppz
						1027	phen
1000		1000	1001		999		bpy
							phz

Table S15. Wavenumber positions (in cm^{-1}) of the Raman bands of complexes **3** and **6**.

FT Raman	3		6	Assignment
	RR at 405 nm	RR at 532 nm	RR at 405/473 nm	
		1603	1605	bpy
1599	1599			dpq
1586	1578	1586	1577	quin
			1561	bpy
1544	1545		1546	dpq
1526	1526		1532	dpq
			1490	bpy
1472	1472	1472	1482	dpq
1438	1438	1439	1444	quin
1386	1388	1387	1387	dpq
1334	1333			
			1318	bpy
1310	1307	1308	1304	quin
			1273	bpy
			1262	phen
	1209		1212	dpq
			1173	bpy
1097				xant
1080				xant
1054		1056	1039	dpq
1029			1027	bpy
1000		1001		

Table S16. Wavenumber positions (in cm^{-1}) of the Raman bands of complexes **4** and **7**.

4	7	Assignment
RR at 405/473 nm	RR at 405/473 nm	
1624	1632	phen
	1605	bpy
1589	1580	phen
1560	1561	bpy
1502	1514	phen
	1488	bpy
1446	1452	phen
1420	1429	phen
1370	1374	phen
	1318	bpy
1303	1307	phen
1293	1297	phen
1262	1274	bpy
1214	1210	phen
	1173	bpy
1146	1147	phen
1100	1110	phen
	1064	phen
1017	1037	phen
	1027	bpy

8 Reductive RR-SEC of complexes 1–7

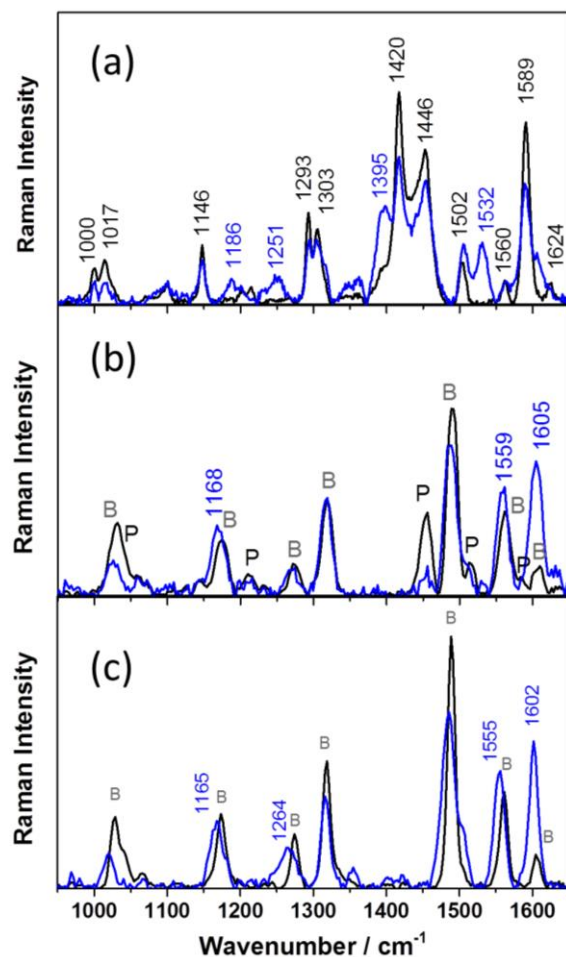


Figure S18. (a) RR spectra of complex **4** (black curves) and singly-reduced **4**⁻ (blue curves) in ACN/ 0.1 M TBAPF₆ solution, excited at 405 nm (upper panel). RR spectra of complex **7** (b) and [Ru(bpy)₃]²⁺ (c) in ACN/ 0.1 M TBAPF₆ solution, excited at 473 nm (upper panel). Characteristic Raman bands of non-reduced **7** are indicated with “P” (for phen ligand) and “B” (for bpy co-ligand).

The RR characterization of Cu(I) complex **4** has been reported previously²⁷, all the strong bands (at 1589, 1560, 1502, 1446, 1420, 1303, 1293, 1146, 1017 and 1000 cm⁻¹ were assigned to the dmp ligands (Figure S16, S18 and Table S16), suggesting the MLCT transitions from Cu to dmp ligand. New bands at 1532 and 1395 cm⁻¹ are observed for singly-reduced **4**⁻ upon 405-nm excitation, which are assigned to the reduced dmp⁻ ligand. The RR spectra of **7** in ACN upon excitation at 405 nm and 473 nm are shown in Figure S17, S18 and Table S16. The characteristic RR bands of bpy co-ligands and phen ligands for **7** are determined by reference compounds

²⁷ Y. Zhang, M. Heberle, M. Wächtler, M. Karnahl, B. Dietzek, *RSC Adv.*, **2016**, *6*, 105801–105805.

$[\text{Ru}(\text{bpy})_3]^{2+}$ and $[\text{Ru}(\text{phen})_3]^{2+28}$. Thus the MLCT_{bpy} transition to bpy is indicated by the intense bands at 1605, 1561, 1488, 1318, 1274, 1173 and 1027 cm^{-1} and the $\text{MLCT}_{\text{phen}}$ transition is relevant to the phen bands at 1513, 1453 and 1210 cm^{-1} . Increased intensity is observed for the RR band at 1605 cm^{-1} , and the bands at 1561 and 1173 cm^{-1} shift to low-frequencies, *i.e.* 1559 and 1168 cm^{-1} . These changes are associated non-reduced bpy ligands due to the charge density changes affected by the radical localized on the phen $^{\bullet-}$ anion. In addition, the phen-based RR bands decrease in intensity upon reduction, *e.g.* bands at 1453 and 1210 cm^{-1} , demonstrating the $\text{MLCT}_{\text{phen}}$ is vanished when one-electron reduction takes place on the phen ligand.

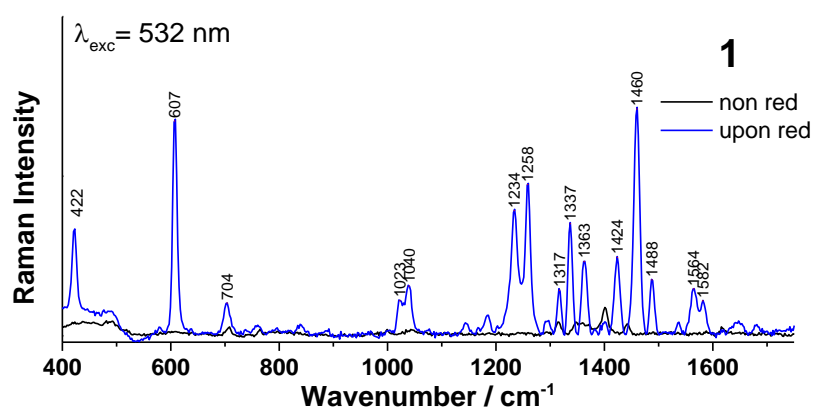


Figure S19. RR spectrum of complex **1** (black curve) and singly-reduced $\mathbf{1}^-$ (blue curve) including the low-frequency region in ACN/ 0.1 M TBAPF₆ solution at 532 nm excitation.

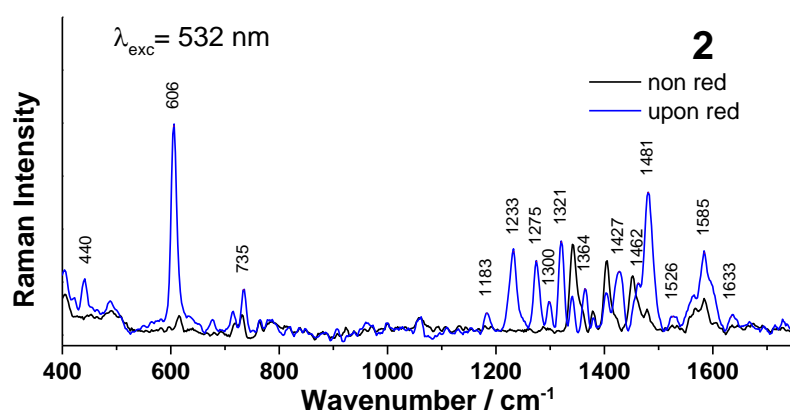


Figure S20. RR spectrum of complex **2** (black curve) and singly-reduced $\mathbf{2}^-$ (blue curve) including the low-frequency region in ACN/ 0.1 M TBAPF₆ solution at 532 nm excitation.

²⁸ J. R. Schoonover, K. M. Omberg, J. A. Moss, S. Bernhard, V. J. Malueg, W. H. Woodruff, T. J. Meyer, *Inorg. Chem.*, **1998**, *37*, 2585–2587.

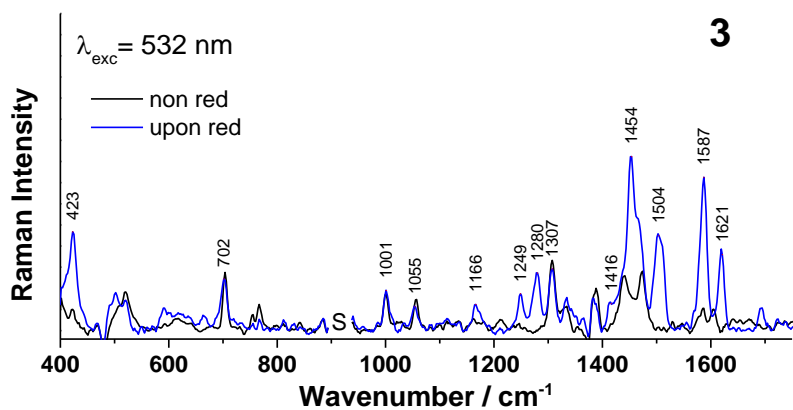


Figure S21. RR spectrum of complex **3** (black curve) and singly-reduced **3⁻** (blue curve) including the low-frequency region in ACN/ 0.1 M TBAPF₆ solution at 532 nm excitation.

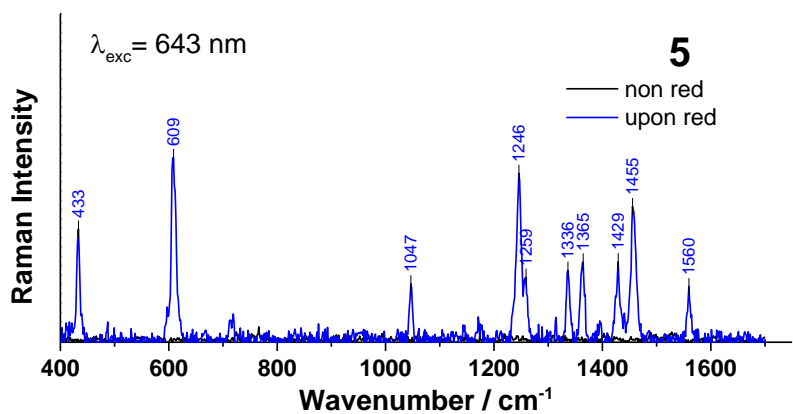


Figure S22. RR spectrum of complex **5** (black curve) and singly-reduced **5⁻** (blue curve) including the low-frequency region in ACN/ 0.1 M TBAPF₆ solution at 643 nm excitation.

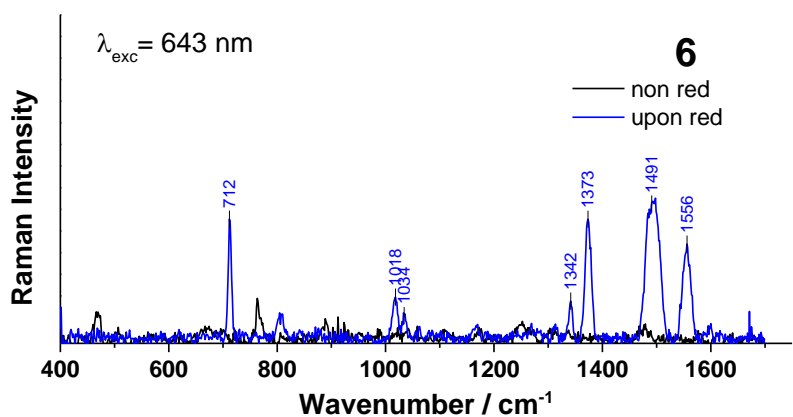


Figure S23. RR spectrum of complex **6** (black curve) and singly-reduced **6⁻** (blue curve) including the low-frequency region in ACN/ 0.1 M TBAPF₆ solution at 643 nm excitation.